

Supplement of:

Evaluation of natural aerosols in CRESCENDO-ESMs: Mineral Dust

Ramiro Checa-Garcia¹, Yves Balkanski¹, Samuel Albani⁸, Tommi Bergman⁵, Ken Carslaw², Anne Cozic¹, Chris Dearden¹⁰, Beatrice Marticorena³, Martine Michou⁴, Twan van Noije⁵, Pierre Nabat⁴, Fionna O'Connor⁷, Dirk Olivie⁶, Joseph M. Prospero⁹, Philippe Le Sager⁵, Michael Schulz⁶, and Catherine Scott²

¹Laboratoire des Sciences du Climat et de l'Environnement, CEA-CNRS-UVSQ, IPSL, Gif-sur-Yvette, France, ²Institute for Climate and Atmospheric Science, School of Earth and Environment, University of Leeds, Leeds, United Kingdom, ³LISA, Universités Paris Est-Paris Diderot-Paris, France, ⁴CNRM-GAME, Météo-France, Centre National de Recherches Météorologiques, UMR3589, 42 avenue G. Coriolis, 31057 Toulouse CEDEX 1, France, ⁵Royal Netherlands Meteorological Institute, De Bilt, Netherlands, ⁶Meteorological Institute, Oslo, Norway, ⁷Met Office Hadley Centre in Exeter, United Kingdom, ⁸Department of Environmental and Earth Sciences, University of Milano-Bicocca, Italy, ⁹Department of Atmospheric Sciences, University of Miami, USA, ¹⁰Centre for Environmental Modelling & Computation (CEMAC), School of Earth & Environment, University of Leeds, UK

Manuscript compiled on November 13, 2020. | Corresponding author: R. Checa-Garcia | ramiro.checa-garcia@lsce.ipsl.fr

List of Figures	3
List of Tables	4
MD: Models and Datasets supplement	5
Datasets: Satellite Retrievals	5
Datasets: Surface Concentrations	8
Datasets: Total Deposition	9
Datasets: INDAAF dataset	9
GL: Global Dust Supplement	12
Global dust cycle	12
Global Dust Budget IPSL-4DU with nudged-winds	17
Comparison of Angstrom Exponent with MISR satellite	17
DE: Dust Emissions supplement	18
Dust Emissions: additional tables	19
Dust Emissions: normalized maps	21
DD: Dust Deposition supplement	22
Dust Deposition: additional tables	23
Dust Wet Deposition: seasonal cycle	25
Dust Deposition: Network of Instruments	31
DOD: Dust Optical Depth supplement	34
Dust Optical Depth: seasonal cycle	35
Dust Optical Depth: skill dust optical depth	41
Seasonal Cycle of AERONETv3 Stations	44
DSC: Dust Surface Concentrations supplement	46
Dust Surface Concentrations: seasonal cycle by regions	47
Seasonal Cycle of Surface Conc. comparison with climatological dataset	53

Network of Surface Concentrations	55
---	----

List of Figures

S.MD.1	Figure: Climatology MODIS-DOD product	6
S.MD.2	Figure: Comparison MODIS dust related products	7
S.MD.3	Figure: Seasonal comparison MODIS dust related products and IASI	7
S.GL.1	Constrains to dust cycle only over land. PD scenario	12
S.GL.2	Constrains to dust cycle only over Sahara & Middle-East. PD scenario	12
S.GL.3	Global maps for CNRM-6DU, CNRM-3DU and UKESM. PI scenario.	13
S.GL.4	Global maps for IPSL, NorESM and EC-Earth. PI scenario.	14
S.GL.5	Global maps for CNRM-6DU, CNRM-3DU. PDN scenario.	15
S.GL.6	Global maps for IPSL and NorESM. PDN scenario.	16
S.GL.8	Comparison of Angstrom Exponent between models and MISR. PD scenario.	17
S.DE.5	Normalised map of emissions (x100) over NorESM grid resolution. PI experiment.	21
S.DD.5	Normalized Seasonal cycle Wet Deposition by regions. PD experiment.	25
S.DD.6	Normalized Seasonal cycle Wet Deposition by regions. PDN experiment.	26
S.DD.7	Normalized Seasonal cycle Wet Deposition by regions. PI experiment.	27
S.DD.8	Seasonal cycle Wet Deposition by regions. PD experiment.	28
S.DD.9	Seasonal cycle Wet Deposition by regions. PDN experiment.	29
S.DD.10	Seasonal cycle Wet Deposition by regions. PI experiment.	30
S.DD.11	CRESCENDO-ESMs against observations to dust deposition (Network-H2011) PI experiment.	31
S.DD.12	CRESCENDO-ESMs against observations to dust deposition (Network-SETB) PI experiment.	32
S.DOD.1	Normalized seasonal cycle Dust Optical Depth by regions. PDN experiment.	35
S.DOD.2	Normalized seasonal cycle Dust Optical Depth by regions. PI experiment.	36
S.DOD.3	Seasonal cycle Dust Optical Depth by regions. PD experiment.	37
S.DOD.4	Seasonal cycle Dust Optical Depth by regions. PDN experiment.	38
S.DOD.5	Seasonal cycle Dust Optical Depth by regions. PI experiment.	39
S.DOD.6	Standard deviation seasonal cycle DOD for multi-model ensemble. PD and PI experiment.	40
S.DOD.7	Spearman based skill of DOD by regions wrt MODIS-DOD. PD experiment.	41
S.DOD.8	Pearson based skill of DOD by regions wrt IASI. PD experiment.	42
S.DOD.9	Spearman based skill of DOD by regions wrt IASI. PD experiment.	43
S.DOD.10	AOD comparison of CNRM-6DU, CNRM-3DU and IPSL over Sahel. PD exp.	44
S.DOD.11	AOD comparison of NorESM and EC-Earth over Sahel. PD exp.	45
S.DSC.1	Normalized Seasonal cycle Dust surface concentrations by regions. PD experiment.	47
S.DSC.2	Normalized Seasonal cycle Dust surface concentrations by regions. PDN experiment.	48
S.DSC.3	Normalized Seasonal cycle Dust surface concentrations by regions. PI experiment.	49
S.DSC.4	Seasonal cycle Dust surface concentrations by regions. PD experiment.	50
S.DSC.5	Seasonal cycle Dust surface concentrations by regions. PDN experiment.	51
S.DSC.6	Seasonal cycle Dust surface concentrations by regions. PI experiment	52
S.DSC.7	Seasonal cycle comparison against observations of dust surface concentrations. PDN experiment .	53
S.DSC.8	Seasonal cycle comparison against observations of dust surface concentrations. PI experiment .	54
S.DSC.10	Comparison against a network of observations of dust surface concentrations. PI experiment . .	55

List of Tables

S.MD.4	Collection of annual dust surface concentrations observations	8
S.MD.5	Collection of total dust deposition fluxes observations	9
S.MD.6	INDAAF dataset stations at Sahel (PM10 surface conc.)	9
S.MD.7	INDAAF dataset stations at Sahel (dust deposition)	9
S.MD.8	DPSD intervals of CRESCENDO-ESMs dust sectional schemes.	10
S.MD.9	DPSD Parameters of CRESCENDO-ESMs dust modal schemes.	10
S.GL.7	Global dust properties for IPSL-4DU model. PDN simulation.	17
S.DE.1	Dust Emission for large regions. PI experiment.	19
S.DE.2	Dust Emission for source regions. PI experiment.	19
S.DE.3	Dust Emission for large regions. PDN experiment.	20
S.DE.4	Dust Emission for source regions. PDN experiment.	20
S.DD.1	Dust Wet Deposition by regions. PI experiment.	23
S.DD.2	Dust Deposition by regions. PDN experiment.	23
S.DD.3	Dust Dry Deposition by regions. PI experiment.	24
S.DD.4	Dust Dry Deposition by regions. PDN experiment.	24
S.DD.13	Statistics of CRESCENDO-ESMs comparison against observations of dust deposition	33
S.DSC.9	Statistics of CRESCENDO-ESMs comparison against observations of dust surface conc.	55

MD: Models and Datasets supplement

This supplement includes additional information about the MODIS-DOD product, following the reference [1], and figures that compares this product with other MODIS based products and IASI. It also have detailed information about ESM-CRESCENDO models properties of mineral dust. Includes the dataset compiled of mineral total dust deposition flux and two tables that summarize the information used from LISA datasets over Sahel. It complement the datasets and model sections of the main paper: *Evaluation of natural aerosols in CRESCENDO-ESMs: Mineral Dust*.

Datasets

Datasets: Satellite Retrievals

IASI dust optical depth

The Infrared Atmospheric Sounder Interferometer (IASI) is a Fourier spectrometer onboard MetOp-A. In contrast with the MISR and MODIS whose measures are focused in the visible, IASI measures in the infrared. We used the IASI dust optical depth product derived from the IASI $10\mu\text{m}$ AOD. Because dust is mostly composed of particles in the coarse-size mode its spectral response cover also infrared channels. The IASI measurements cover altitudes that are considerably higher than the first hundred meters over the ocean where most of the mass of sea-salt aerosols resides. Therefore it is possible to ascertain dust coarse optical depth [2] from IASI $10\mu\text{m}$ AOD. The dataset covers the time-interval Jul-2007 to Dec-2014. Because IASI gives an estimation of dust optical depth at infrared, but not at 550 nm like model diagnostic. The figure S.MD.3 compares this product with MODIS DOD products. Note that it is possible to reconstruct a confidence interval of IASI product at 550 nm by implementing the range of conversion factor shown by [6]. However the actual factors \mathcal{F} depend on the mineralogy composition of dust and the actual size distribution with a typical range: $0.35 \leq \mathcal{F} \leq 0.55$.

MODIS dust products

MODIS Filter

If the results of 3 filters applied to MODIS deepblue aerosol product

- $\alpha < 1.4$
- $\omega_{412nm} < 0.95$
- $\tau_{412nm} - \tau_{660nm} > -0.02$

Then the MODIS optical depth τ_{550nm} values for aerosols is considered dominated by dust optical depth $\tau_{DOD-550nm}$

MODIS Filter-B

To test the sensitivity of this filter another has been created the final product is also $\tau_{DOD-550nm}$.

- $\alpha < 1.49$
- $\omega_{412nm} < 0.95$
- $\tau_{412nm} - \tau_{660nm} > -0.05$

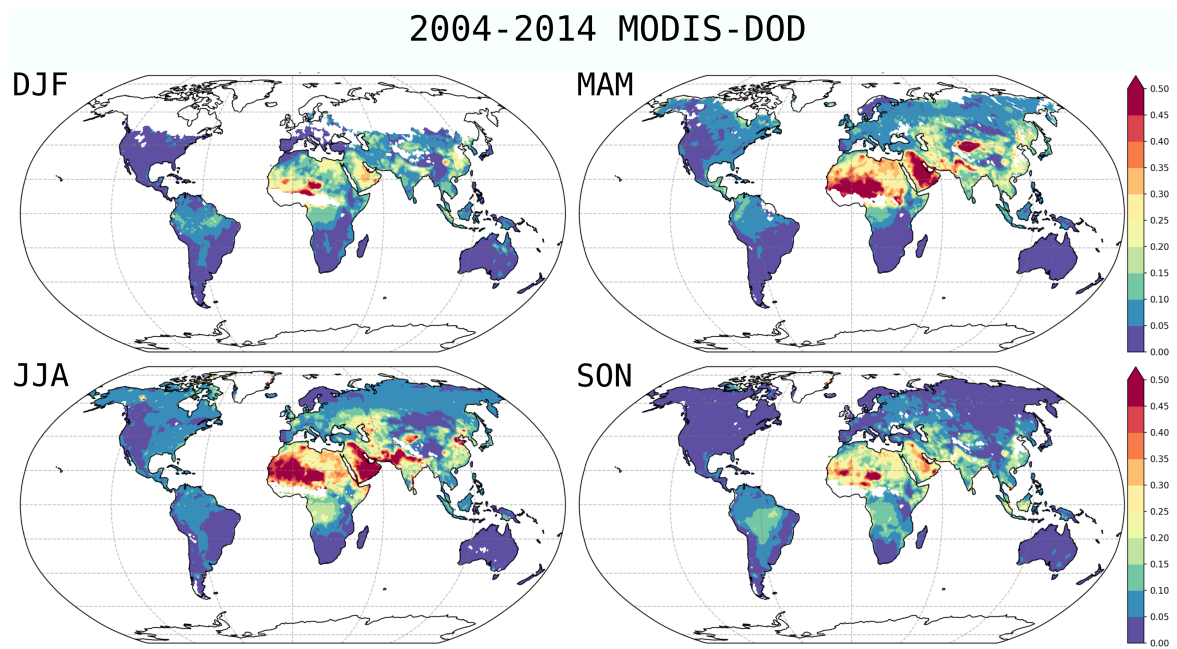


Figure S.MD.1: Climatology of MODIS-DOD product based on monthly level 3 collection 6.1. The seasonality, regional patterns and values are consistent with reference [8].

MODIS DOD

This product relies on an re-scaling of the aerosol optical depth based on a formula given by [8] together with the filter:

- $\omega_{412nm} < 0.97$
- $\tau_{DOD-550nm} = \tau_{550nm}(0.98 - 0.5089\alpha + 0.0512\alpha^2)$

The DOD is approximated as $\tau_{DOD-550nm} = \tau_{550nm}(0.98 - 0.5089\alpha + 0.0512\alpha^2)$, as this equation has been analysed for MODIS deepblue 6.1 with daily resolution [8]. We implemented over a monthly resolution and compared the seasonal properties with the Figure 1 of [8]. The global distribution and value intervals are consistent for regional and seasonal/monthly analysis with only slight differences over China and Oceania (region not included on our analysis), although maximum values are located in the same locations with close values, see Figure S.MD.1.

The Figure S.MD.2 shows comparative maps of the filters for the years 2006, 2008 and 2010, 2012. MODIS-Filter and MODIS-FilterB have similar pattern but the last is less strict filtering the dusty pixels. However, both perform well as they have signatures of dust emissions on the source regions analysed on the main paper. The MODIS-DOD instead is less strict on the source regions being potentially able to detect signatures of dust on regions not directly characterized to be dust sources. Its comparison with the last column at S.MD.2 indicates that the original τ_{550nm} is effectively decreased on most of the regions, and the S.MD.3 shows that the seasonal cycle of MODIS-Filters and MODIS-DOD is the same but the re-scaling decrease the values of MODIS-DOD consistently for all the seasons. IASI dust optical depth product shows different values as it represents the optical depth at $10\mu m$, while the seasonality is consistent for African and Middle East regions, with only remarkable differences at Taklamakan.

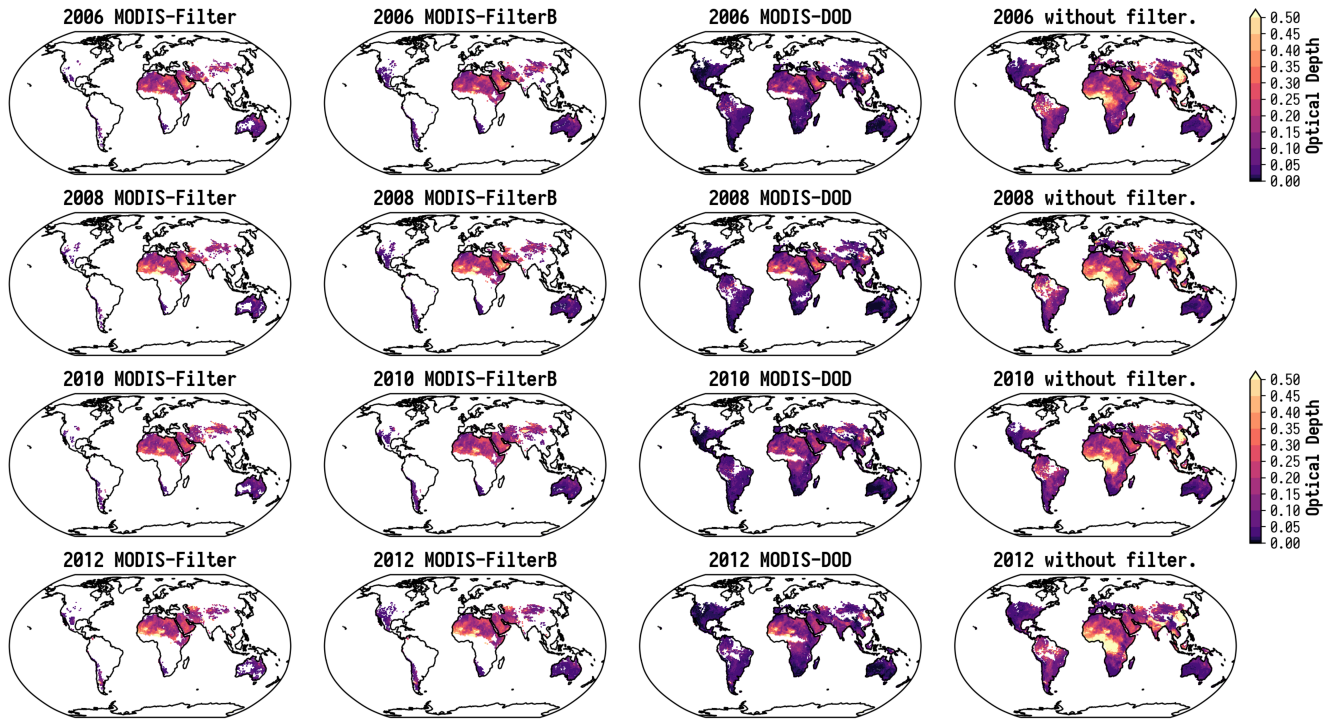


Figure S.MD.2: Comparison of the three MODIS dust related products for the same years 2006, 2008, 2010 and 2012. The last column indicate the MODIS aerosol optical depth over land without any custom filtering or scaling.

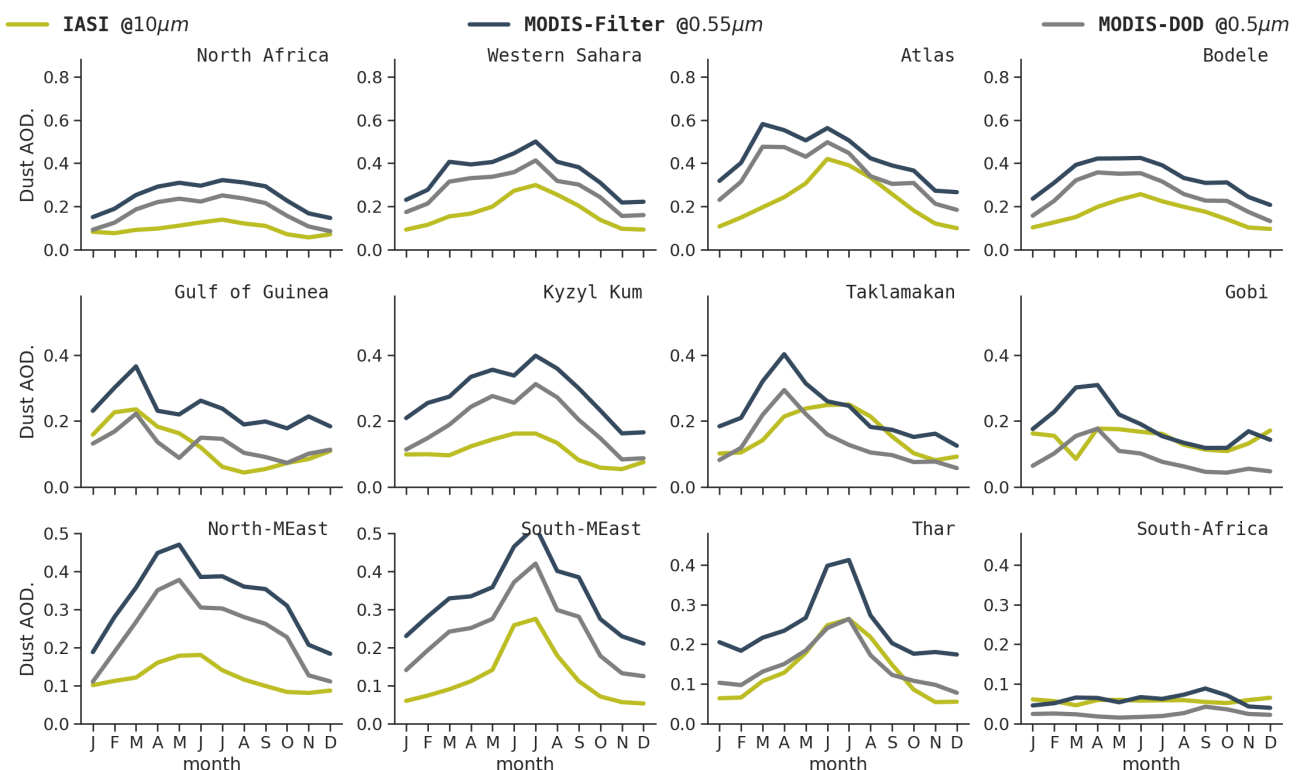


Figure S.MD.3: Comparison of seasonal optical depths of MODIS related products with IASI for regions with larger dust optical depths. The DOD retrieval from IASI is in the infrared (at $10\mu\text{m}$) therefore the values are expected to be smaller but with consistent seasonal variability [7, 6]. Period 2007-2014 due to IASI dataset availability.

Datasets: Surface Concentrations

Station Number	Station Name	Latitude	Longitude	Surface Concentration	Reference	Region
1	Tillabery-Mali	14.2	1.5	48.4	[1]	NorthAfrica
2	Hong Kong	22.3	114.2	20.029	[1]	Asia
3	Canary Islands	29.2	-13.5	63.486	[1]	NorthAfrica
4	Eilat-Israel	29.5	34.8	30.829	[1]	MiddleEast
5	Sede Boker-Israel	30.9	34.8	35.629	[1]	MiddleEast
6	Tel Shikmona-Israel	32.8	35	21.7	[1]	MiddleEast
7	Grand Canyon-USA	36.0	-112	3.571	[1]	NorthAmerica
8	Erdemli-Turkey	36.5	34.3	10.3	[1]	Mediterranean
9	NOSE: Texel-Netherlands	53.1	4.8	4.994	[1]	Europe
10	NOSE: Alkor-Belgica	54.7	7.2	3.371	[1]	Europe
11	FPN	55	4	1.523	[1]	Europe
12	King George	-62.18	-58.3	0.613 (0.52)	[1]	Antartica
13	Cape Grim-Australia	-40.68	144.68	1.248	[1]	Australia
14	Cape Point-S.Africa	-34.35	18.48	2.225 (2.20)	[1]	SouthAfrica
15	Norfolk Island	-29.08	167.98	0.884 (0.84)	[1]	Australia
16	Midway-Hawaii	28.22	-177.35	0.819 (0.72)	[1]	PacificOcean
17	New Caledonia (Yate)	-22.15	167	0.173 (0.17)	[1]	Australia
18	American Samoa	-13.5	-172.5	0.02 (0.16)	[1]	PacificOcean
19	Funafuti	-8.5	179.2	0.169 (0.19)	[1]	PacificOcean
20	Nauru	-0.5	166.9	0.106 (0.10)	[1]	PacificOcean
21	Fanning	3.9	159.3	0.06 (0.10)	[1]	PacificOcean
22	Enewetak	11.3	162.3	0.247 (0.24)	[1]	PacificOcean
23	Barbados	13.17	-59.43	16.256(14.48)	[1]	AtlanticOcean
24	Cape Verde	16.7	-22.9	43.087	[1]	AtlanticOcean
25	Oahu-Hawaii	21.33	-157.7	0.64 ((0.66)	[1]	PacificOcean
26	Hedo-Korea	26.92	128.25	9.147	[1]	Asia
27	Miami-USA	27.75	-80.25	6.716 (4.59)	[1]	NorthAmerica
28	Izana-Tenerife	28.3	-16.5	25.518 (30.18)	[1]	AtlanticOcean
29	Bermuda	32.27	-64.87	3.193 (3.36)	[1]	AtlanticOcean
30	Cheju-Korea	33.52	126.48	15.99 (14.14)	[1]	Asia
31	Wajima-Japan	37.3	136.9	13.75	[1]	Asia
32	Niigata	37.9	139.1	18.75	[1]	Asia
33	Okushiri-Japan	42.1	139.1	25	[1]	Asia
34	Sapporo	43.1	141.3	30	[1]	Asia
35	Shemya	52.7	174	0.89	[1]	PacificOcean
36	Mace Head-Ireland	53.3	-9.9	0.509	[1]	Europe
37	Mawson-Antarctica	-67.6	62.5	0.10	[3]	Antarctica
38	Palmer St. Antarctica	-64.8	-64.1	0.35	[3]	Antarctica
39	Rarotonga-Cook Islands	-21.2	-159.8	0.11	[3]	PacificOcean
40	Hedo-Okinawa-Japan	29.6	128.2	8.37	[3]	Asia

Table S.MD.4: Table with the climatology of annual surface concentration of dust μgm^{-3} . When both references [3] and [1] report values on the same station we used the most recent reference value [1] but the values of [3] are given between parenthesis.

Datasets: Total Deposition

Station Number	Station Name	Location (Lat,Lon)	Deposition [$g m^{-2} yr^{-1}$]	Region	Reference
1	CapFerrat	43.69 N,7.33 E	11.4	W-Mediterranean	[9]
2	CapBear	42.512 N,3.14 E	10.6	W-Mediterranean	[9]
3	CapCavallo	42.52 N,8.77 E	12.5	W-Mediterranean	[9]
4	Ostriconi	42.66 N,9.06 E	27.4	W-Mediterranean	[9]
5	CapCarbonara	39.1 N,9.5 E	12.8	W-Mediterranean	[9]
6	Lanjaron	36.91 N,3.48 W	11.1	W-Mediterranean	[9]
7	Akkuyu	36.14 N,33.54 E	10.1	E-Mediterranean	[9]
8	Finokalia	35.33 N,25.67 E	8.8	E-Mediterranean	[9]
9	CavoGreco	34.96 N,34.06 E	4.2	E-Mediterranean	[9]
10	Mytilene	39.10 N,26.56 E	5.4	E-Mediterranean	[9]
11	Alexandria	31.2 N,29.92 E	20.3	Egypt	[9]
12	CapSpartel	35.79 N,5.93 W	7.2	Maghreb	[9]
13	Mahdia	35.33 N,10.89 E	23.3	Maghreb	[9]
14	Gefara	32.45 N,12.94 E	215	Libya	[5]
15	Misrata	32.33 N,15.10 E	105	Libya	[5]
16	CentralLibya	29.00 N,16.70 E	276	Libya	[5]
17	SouthernLibya	27.25 N,14.50 E	82	Libya	[5]
18	Banizoumbou	13.45 N,2.66 E	134.65	Sahel	[4]
19	Cinzana	13.28 N,5.93 W	121.9	Sahel	[4]
20	MBour	14.38 N,16.96 W	94.0	Sahel	[4]

Table S.MD.5: Table with the climatology of deposition fluxes over Mediterranean and Sahel regions. Those measurements are extracted from the given publications. For the reference [4] the values has been estimated from the time interval 2007-2011.

Datasets: INDAAF dataset

Station	Period	Country	Location	PM10 Surface Conc.		
				Avg	Max	Min
Banizoumbou	03-2007/11-2011	Niger	(13.54N, +02.66E)	173.7	611.1	15.2
Cinzana	02-2007/12-2011	Mali	(13.28N, -05.93E)	119.9	375.1	13.3
M'Bour	07-2007/12-2011	Senegal	(14.39N, -16.96E)	107.7	262.1	30.9

Table S.MD.6: Global properties of the three stations used from the INDAAF dataset for averaged, maximum and minimum values surface concentrations of PM10 [$\mu g m^{-3}$]. Source: [4].

Station	Period	Country	Location	Total Deposition			Wet-Deposition			Dry-Deposition		
				Avg	Max	Min	Avg	Max	Min	Avg	Max	Min
Banizoumbou	03-2007/11-2011	Niger	(13.54N, +02.66E)	134.6	155.7	93.6	67.1	117.6	38.0	49.0	82.9	35.2
Cinzana	02-2007/12-2011	Mali	(13.28N, -05.93E)	121.9	159.9	75.3	77.4	117.0	51.4	36.7	66.2	20.9
M'Bour	07-2007/12-2011	Senegal	(14.39N, -16.96E)	94.0	102.1	79.1	6.26	8.90	4.70	70.4	87.4	56.1

Table S.MD.7: Global properties of the three stations used from the INDAAF dataset for averaged, maximum and minimum values of total, wet, dry depositions [$gm^{-2} yr^{-1}$] of PM10 [$\mu g m^{-3}$]. Source: [4].

Models

Models: Information about DPSD

Bin	CNRM-6DU	CNRM-3DU	UKESM
1	[0.05, 0.10]	[0.005, 0.50]	[0.0316, 0.100]
2	[0.10, 0.25]	[0.500, 1.25]	[0.1000, 0.316]
3	[0.25, 0.50]	[1.250, 10.00]	[0.3160, 1.000]
4	[0.50, 1.25]	-	[1.0000, 3.160]
5	[1.25, 5.00]	-	[3.1600,10.000]
6	[5.00,50.00]	-	[10.000,31.600]

Table S.MD.8: Bin intervals for CNRM-6DU, CNRM-3DU and UKESM models. The size is represented by the geometric radius of the dust particle in μm .

IPSL	EC-Earth	NorESM	IPSL-4DU
-	(0.5, 1.59)	(0.44,2.00)	(1.00, 1.8) $\rightarrow m_1$
(2.5, 2.00)	(2.0, 2.00)	(1.26,2.10)	(2.50, 2.0) $\rightarrow m_{2.5}$
-	-	-	(7.00, 1.9) $\rightarrow m_7$
-	-	-	(22.0, 2.0) $\rightarrow m_{22}$

Table S.MD.9: Parameters that define the shape and location of lognormal modes of dust particle size distribution. Each mode is described by two parameters: one describing an initial characteristic size at emission in μm and the other describing the width of the distribution, so we report the part of values (D_m, σ) , where D_m is the mass median diameter. In the case of ECv3 dust is part of a mixed mode. For the IPSL with 4 dust modes, the mode names are also given in the table.

References of Supplement MD

- [1] S. Albani, N. M. Mahowald, A. T. Perry, R. A. Scanza, C. S. Zender, N. G. Heavens, V. Maggi, J. F. Kok, and B. L. Otto-Bliesner. "Improved dust representation in the Community Atmosphere Model". In: *Journal of Advances in Modeling Earth Systems* 6 (2014), pp. 541–570. DOI: <https://doi.org/10.1002/2013MS000279>.
- [2] V. Capelle, A. Chédin, M. Siméon, C. Tsamalis, C. Pierangelo, M. Pondrom, C. Crevoisier, L. Crepeau, and N. A. Scott. "Evaluation of IASI-derived dust aerosol characteristics over the tropical belt". In: *Atmospheric Chemistry and Physics* 14.17 (2014), pp. 9343–9362. DOI: 10.5194/acp-14-9343-2014. URL: <https://www.atmos-chem-phys.net/14/9343/2014/>.
- [3] T. Cheng, Y. Peng, J. Feichter, and I. Tegen. "An improvement on the dust emission scheme in the global aerosol-climate model ECHAM5-HAM". In: *Atmospheric Chemistry and Physics* 8.4 (Feb. 2008), pp. 1105–1117. DOI: 10.5194/acp-8-1105-2008. URL: <https://doi.org/10.5194/acp-8-1105-2008>.
- [4] B. Marticorena, B. Chatenet, J. L. Rajot, G. Bergametti, A. Deroubaix, J. Vincent, A. Kouoi, C. Schmechtig, M. Coulibaly, A. Diallo, I. Koné, A. Maman, T. NDiaye, and A. Zakou. "Mineral dust over west and central Sahel: Seasonal patterns of dry and wet deposition fluxes from a pluriannual sampling (2006–2012)". In: *Journal of Geophysical Research: Atmospheres* 122.2 (2017), pp. 1338–1364. DOI: 10.1002/2016JD025995. eprint: <https://agupubs.onlinelibrary.wiley.com/doi/pdf/10.1002/2016JD025995>. URL: <https://agupubs.onlinelibrary.wiley.com/doi/abs/10.1002/2016JD025995>.
- [5] Sarah L. O'Hara, Michèle L. Clarke, and Mokhtar S. Elat rash. "Field measurements of desert dust deposition in Libya". In: *Atmospheric Environment* 40.21 (2006), pp. 3881–3897. ISSN: 1352-2310. DOI: <https://doi.org/10.1016/j.atmosenv.2006.02.020>. URL: <http://www.sciencedirect.com/science/article/pii/S1352231006002305>.
- [6] S. Peyridieu, A. Chédin, V. Capelle, C. Tsamalis, C. Pierangelo, R. Armante, C. Crevoisier, L. Crépeau, M. Siméon, F. Ducos, and N. A. Scott. "Characterisation of dust aerosols in the infrared from IASI and comparison with PARASOL, MODIS, MISR, CALIOP, and AERONET observations". In: *Atmospheric Chemistry and Physics* 13.12 (2013), pp. 6065–6082. DOI: 10.5194/acp-13-6065-2013. URL: <https://www.atmos-chem-phys.net/13/6065/2013/>.
- [7] S. Peyridieu, A. Chédin, D. Tanré, V. Capelle, C. Pierangelo, N. Lamquin, and R. Armante. "Saharan dust infrared optical depth and altitude retrieved from AIRS: a focus over North Atlantic: comparison to MODIS and CALIPSO". In: *Atmospheric Chemistry and Physics* 10.4 (2010), pp. 1953–1967. DOI: 10.5194/acp-10-1953-2010. URL: <https://www.atmos-chem-phys.net/10/1953/2010/>.
- [8] B. Pu and P. Ginoux. "How reliable are CMIP5 models in simulating dust optical depth?" In: *Atmospheric Chemistry and Physics* 18.16 (2018), pp. 12491–12510. DOI: 10.5194/acp-18-12491-2018. URL: <https://www.atmos-chem-phys.net/18/12491/2018/>.
- [9] J. Vincent, B. Laurent, R. Losno, E. Bon Nguyen, P. Roullet, S. Sauvage, S. Chevaillier, P. Coddeville, N. Ouboulmane, A. G. di Sarra, A. Tovar-Sánchez, D. Sferlazzo, A. Massanet, S. Triquet, R. Morales Baquero, M. Fornier, C. Coursier, K. Desboeufs, F. Dulac, and G. Bergametti. "Variability of mineral dust deposition in the western Mediterranean basin and south-east of France". In: *Atmospheric Chemistry and Physics* 16.14 (2016), pp. 8749–8766. DOI: 10.5194/acp-16-8749-2016. URL: <https://www.atmos-chem-phys.net/16/8749/2016/>.

GL: Global Dust Supplement

This supplement includes additional information for the sections 4.1 and 4.2 of main paper *Evaluation of natural aerosols in CRESCENDO-ESMs: Mineral Dust*.

Global dust cycle

This section complements the **Figure 4** of the main manuscript by showing the inter-annual variability with boxed plots, together with filtering the variables over two regions: land and Sahara & Middle-East (the filters constrain the mean fields over specific regions). The rationale of land filter analysis is to don't account regions with low values of loadings that can drive high-values of global mass extinction efficiency (MEE), whereas the Sahara & Middle-East region is focused on evaluate constraints over an area where aerosol dust emissions are dominant.

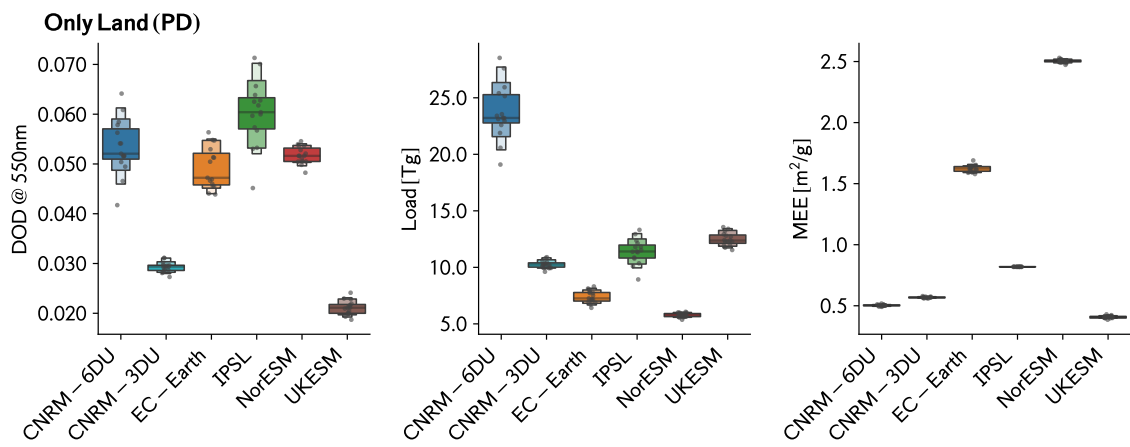


Figure S.GL.1: Constraints to dust cycle only over land. The boxen-plot represents the annual variability from 2000-2014. Scenario PD. The variability of MEE is significantly smaller than loadings and dust optical depths

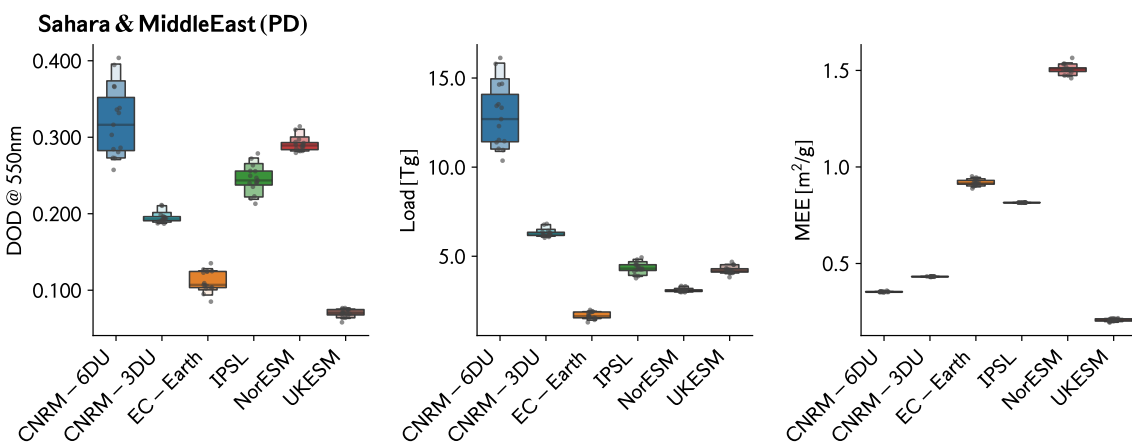


Figure S.GL.2: Constraints to dust cycle only over a Sahara & Middle-East. The boxen-plot represents the annual variability from 2000-2014. Scenario PD. The variability of MEE is significantly smaller than loadings and dust optical depths

PI experiment

These figures are the equivalents of *Figures 5 and 6* in main manuscript but for the PI scenario. The figure S.GL.3, has the three models with bin/sectional schemes. The figure S.GL.4 those models with modal description of mineral dust. The results are in agreement with PD scenario although CNRM-5DU model present large variations of mass extinction efficiency.

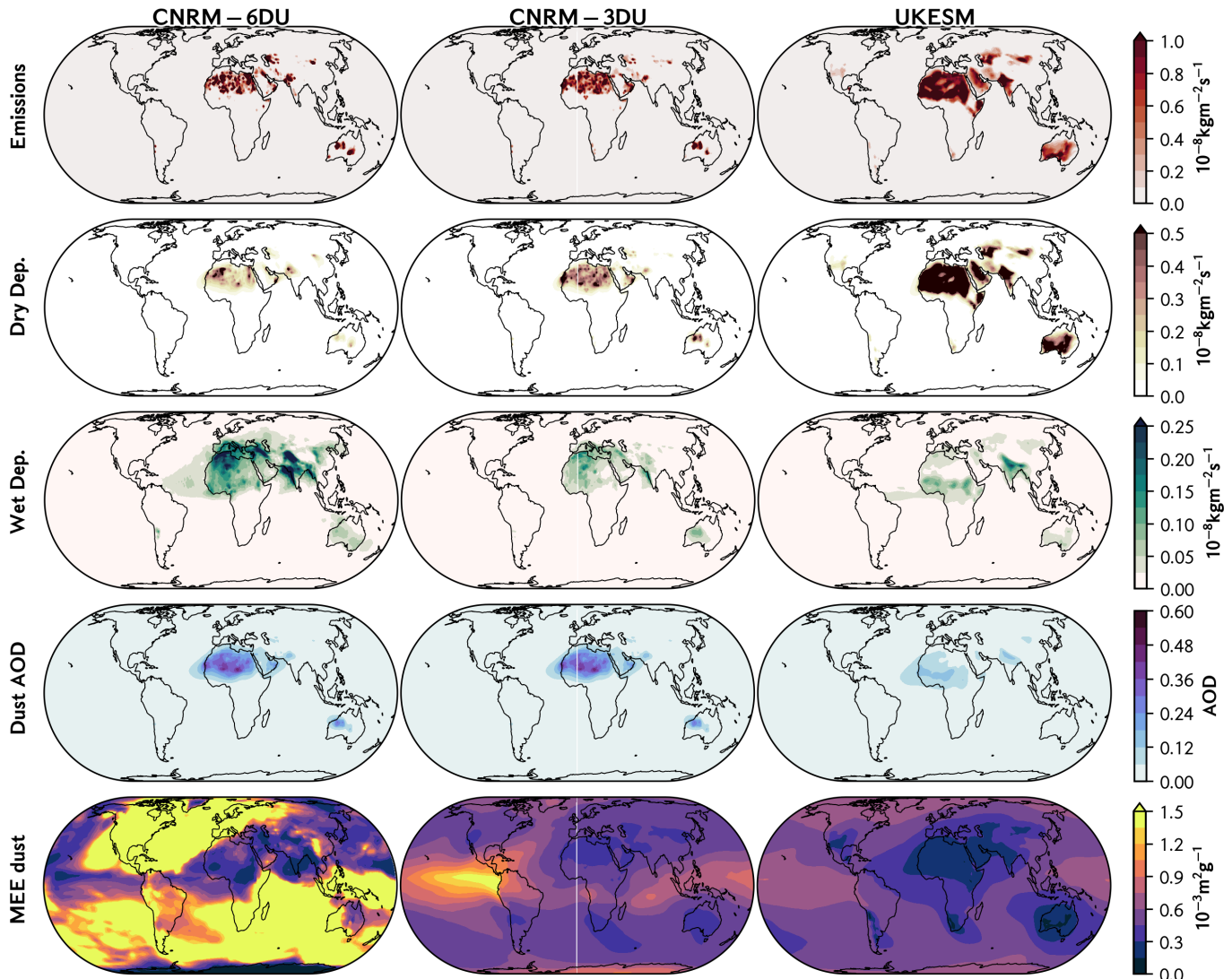


Figure S.GL.3: CRESCENDO-ESMs maps, PI scenario, describing dust properties: emission tendency, depositions tendencies, dust optical depths and mass extinction efficiency. Models CNRM-6DU, CNRM-3DU and UKESM models (bins based dust parametrization).

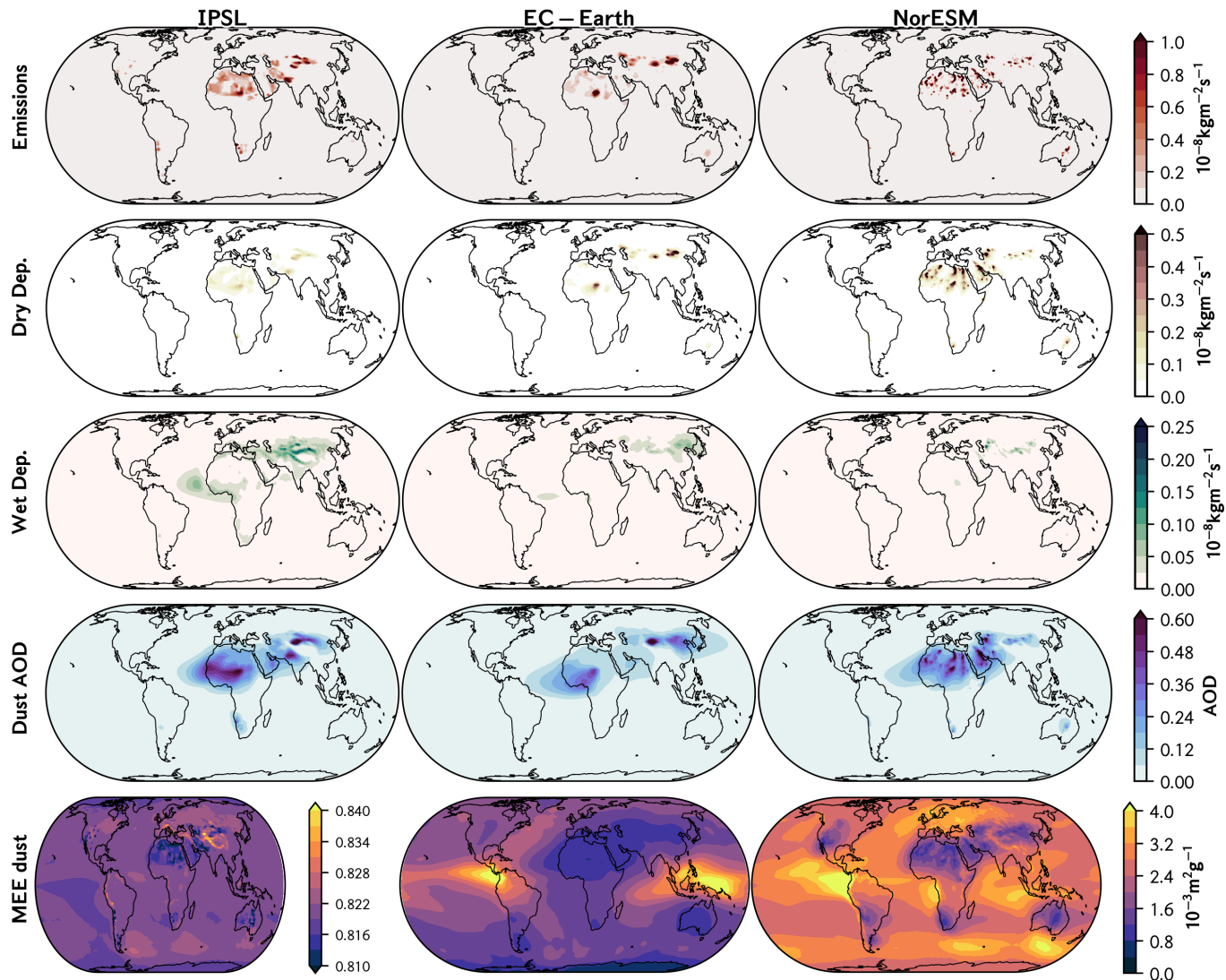


Figure S.GL.4: CRESCENDO-ESMs maps, PI scenario, describing dust properties: emission tendency, depositions tendencies, dust optical depths and mass extinction efficiency. Models IPSL, NorESM and EC-Earth models (modal based dust parametrization).

PDN experiment

These figures are the equivalents of *Figures 5 and 6* in main manuscript but for the PDN scenario. The figure S.GL.5 has the CNRM models (bin/sectional schemes). The figure S.GL.6 the IPSL and NorESM models, both with modal description of mineral dust.

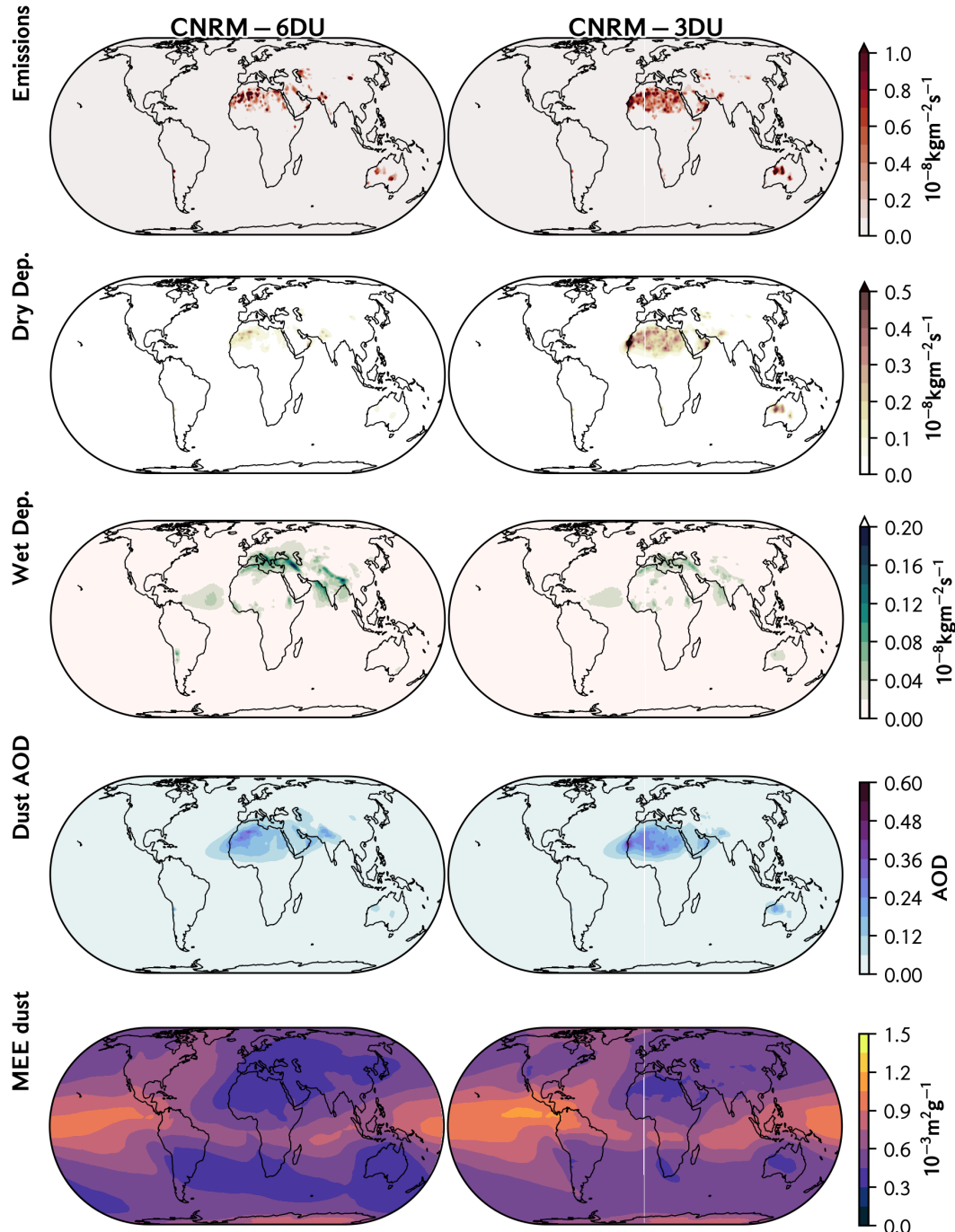


Figure S.GL.5: CRESCENDO-ESMs maps, PDN scenario, describing dust properties: emission tendency, depositions tendencies, dust optical depths and mass extinction efficiency. Models CNRM-6DU, CNRM-3DU (bins based dust parametrization).

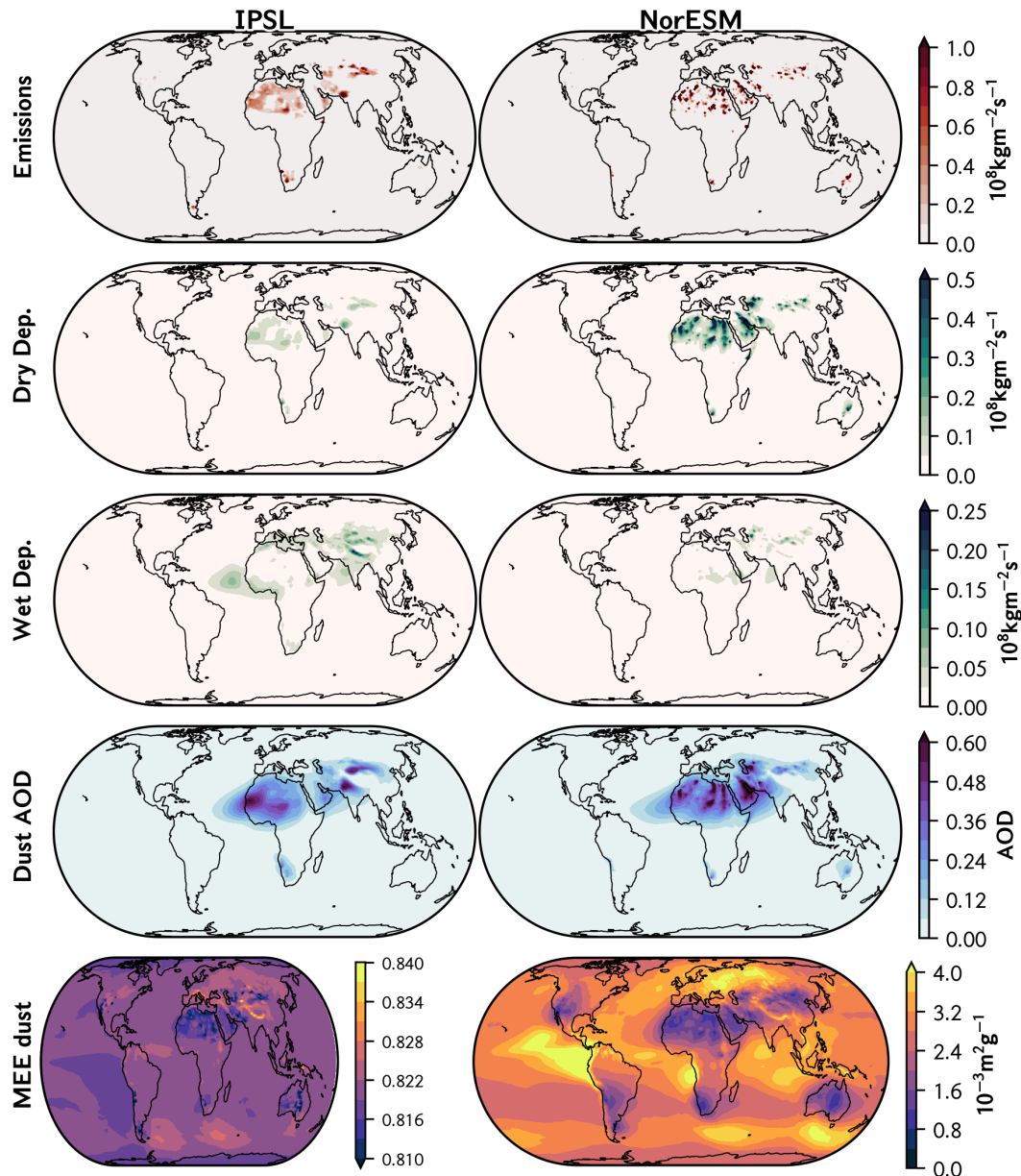


Figure S.GL.6: CRESCENDO-ESMs maps, PDN scenario, describing dust properties: emission tendency, depositions tendencies, dust optical depths and mass extinction efficiency. Models IPSL-INCA and NorESM (modal based dust parametrization).

Global Dust Budget IPSL-4DU with nudged-winds

IPSL-Mode	Emissions [Tg/yr]	Dry Dep. [Tg/yr]	Wet Dep. [Tg/yr]	Sedim. [Tg/yr]	\mathcal{R}_{dep}	Loadings [Tg]	DOD 550nm -
Mode m ₁	94.3	22.8	68.9	2.5	0.37	1.39	0.005
Mode m _{2.5}	691.3	156.9	411.4	122.4	0.68	8.21	0.012
Mode m ₇	5098.6	765.9	1282.3	3048.0	2.97	27.5	0.011
Mode m ₂₂	10316.2	370.9	231.5	9713.4	432	6.75	0.0009

Table S.GL.7: Global properties of the dust scheme with 4 modes implemented in IPSL [1] for an experiment with nudged-winds (PDN). \mathcal{R}_{dep} is the ratio of total dry deposition (with sedimentation) over wet deposition. This dust scheme includes 3 additional modes to the default IPSL scheme. Additionally it is including both number concentration and mass concentration for each mode, therefore the additional dust modes are not mixed in with other species inside a mode.

Comparison of Angstrom Exponent with MISR satellite

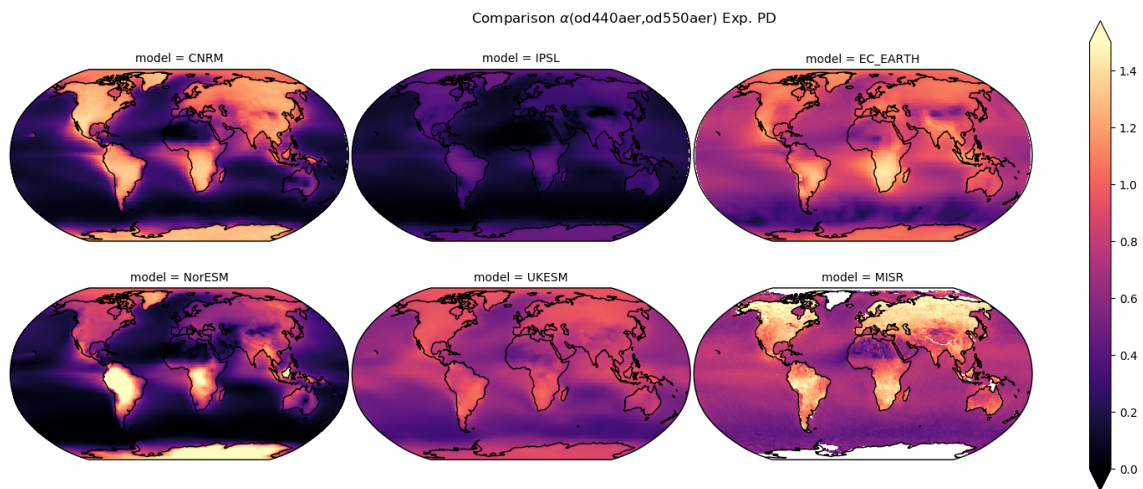


Figure S.GL.8: Comparison of Angstrom Exponent calculated from optical depths at 440nm and 550nm for CRESCENDO-ESMs and MISR satellite dataset using the same methodology. PD scenario.

References of Supplement Global Dust (GL)

- [1] Samuel. Albani and et-al. “The global dust cycle in the IPSL climate model revisited: particle size distributions and dependence of emissions on land surface properties”. In: *in preparation* (2020).

DE: Dust Emissions supplement

This supplement includes additional information for the sections 4.3 main paper *Evaluation of natural aerosols in CRESCENDO-ESMs: Mineral Dust.*

Dust Emissions: additional tables

This section complements the **Table 5** of the main manuscript with the equivalent tables for PDN and PI experiments.

Table S.DE.1 Equivalent of Table 5 (global part) of main paper for PI experiment.

Table S.DE.3 Equivalent of Table 5 (global part) of main paper for PDN experiment.

Table S.DE.2 Equivalent of Table 5 (regions part) of main paper for PI experiment.

Table S.DE.4 Equivalent of Table 5 (regions part) of main paper for PDN experiment.

Dust Emissions: normalized maps

This section complements the **Figure 7** of the main manuscript with the equivalent tables for PDN and PI experiments.

Fig. S.DE.5 Equivalent of Figure 7 of main paper for PI experiment.

Dust Emissions: additional tables

Table S.DE.1: Emissions [$Tg\ yr^{-1}$] for Pre-Industrial (PI) experiment. Globally and over Land/Coastlines. (*) Denotes those models with bin sizes larger than $10\mu m$. Sahara desert emissions and its percentage over total emissions is obtained from the sum of the regions: Western Sahara, Mali, Bodele and North Sahara, so it is not including Sahel.

	CNRM-6DU (PI)	CNRM-3DU (PI)	EC-Earth (PI)	IPSL (PI)	NorESM (PI)	UKESM (PI)
Global Earth	3887.3	(*)	2651.5	(*)	1145.8	1551.7
Land	3700.4	(*)	2567.7	(*)	1129.5	1544.5
Ocean (Coast)	187.0	(*)	83.8	(*)	16.3	7.3
Sahara Desert	2267.4	(58%)	1755.9	(66%)	421.9	(37%)
North. Hemis.	3488.4	(90%)	2333.9	(88%)	1087.3	(95%)
South. Hemis.	398.9	(10%)	317.6	(12%)	58.5	(5%)
					1407.3	7421.9
					1382.5	7404.4
					24.7	17.5
					664.4	(47%)
					1296.9	(92%)
					4283.3	(58%)
					6496.3	(88%)
					110.4	(8%)
					925.6	(12%)

Table S.DE.2: Emissions [$Tg\ yr^{-1}$] for PI experiment. Over 15 different regions. In brackets the order of the 9 regions with largest emissions.

	CNRM-6DU (PI)	CNRM-3DU (PI)	EC-Earth (PI)	IPSL (PI)	NorESM (PI)	UKESM (PI)
South-America	16.7	13.4	11.0	33.6	9.2	18.3
South-Africa	6.7	17.3	2.5	87.7	(7)	32.2
Australia	333.0	(4)	239.9	(5)	40.6	(9)
Mali/Niger	400.5	(3)	328.2	(3)	43.0	(7)
Western Sahara	246.3	(6)	297.7	(4)	45.2	(6)
Bodele/Sudan	650.7	(2)	572.9	(1)	244.0	(2)
North Africa	969.9	(1)	557.1	(2)	89.7	(5)
North-MiddleEast	262.5	(5)	114.3	(8)	20.7	40.2
South-MiddleEast	217.6	(9)	205.7	(6)	40.8	(8)
Kyzyl Kum	221.1	(8)	122.9	(7)	121.6	(3)
Thar	238.0	(7)	58.5	(9)	155.6	(4)
Taklamakan	18.7		15.4		97.7	(6)
Gobi	162.6		36.7		160.9	(3)
North-America	0		1.2		112.0	(5)
					214.2	(2)
					27.6	6.1
					369.8	(7)
					16.2	273.1
					38.1	(9)
					75.4	
					86.0	(6)
					223.9	
					54.9	

Table S.DE.3: Emissions [$Tg\ yr^{-1}$] for PDN simulations. Globally and over Land/Coastlines. (*) Denotes those models with bin sizes larger than $10\mu m$. Sahara desert emissions and its percentage over total emissions is obtained from the sum of the regions: Western Sahara, Mali, Bodele and North Sahara, so it is not including Sahel.

	CNRM-6DU (PDN)	CNRM-3DU (PDN)	IPSL (PDN)	NorESM (PDN)
Global Earth	1278.4	(*)	1812.1	(*)
Land	1213.5	(*)	1743.3	(*)
Ocean (Coast)	64.9	(*)	68.8	(*)
Sahara Desert	735.1	(57%)	1180.0	(65%)
North. Hemis.	1141.3	(89%)	1589.1	(88%)
South. Hemis.	137.1	(11%)	223.0	(12%)
			1295.3	1733.6
			1271.3	1696.1
			24.0	37.4
			663.9	(51%)
			1161.6	(89%)
			810.0	(47%)
			1596.1	(92%)
			133.7	(11%)
			137.5	(8%)

Table S.DE.4: Emissions [$Tg\ yr^{-1}$] for Present Day (PDN) simulations. Over 15 different regions. In brackets the order of the 9 regions with largest emissions.

	CNRM-6DU (PDN)	CNRM-3DU (PDN)	IPSL (PDN)	NorESM (PDN)
South-America	21.7	13.6	20.3	11.0
South-Africa	2.4	14.0	92.2	(8) 40.9
Australia	97.7	(5)	162.3	(5) 12.1 71.6 (9)
Mali/Niger	120.1	(3)	201.1	(4) 83.4 (9) 72.3 (8)
Western Sahara	125.2	(2)	263.5	(3) 118 (3) 147.2 (5)
Bodele/Sudan	119.6	(4)	325.6	(2) 210.7 (2) 215 (3)
North Africa	370.2	(1)	389.8	(1) 221.8 (1) 375.5 (1)
North-MiddleEast	89.1	(7)	77.3	(8) 29.1 208.9 (4)
South-MiddleEast	73.2	(8)	149.3	(6) 64.5 118.2 (6)
Kyzyl Kum	91.9	(6)	85.4	(7) 107.8 (4) 240.7 (2)
Thar	64.7	(9)	47.9	(9) 101.5 (5) 22.7
Taklamakan	4.9		10.4	
Gobi	45.9		22.5	
North-America	0		1.1	
			18.3	5.9

Dust Emissions: normalized maps

As commented on the main text a direct comparison of the normalized emission maps with observations need to translate the observed frequency of dust events into a dust emission flux rate [1]. However still it is possible to compare the qualitative location of hot-spots over different regions.

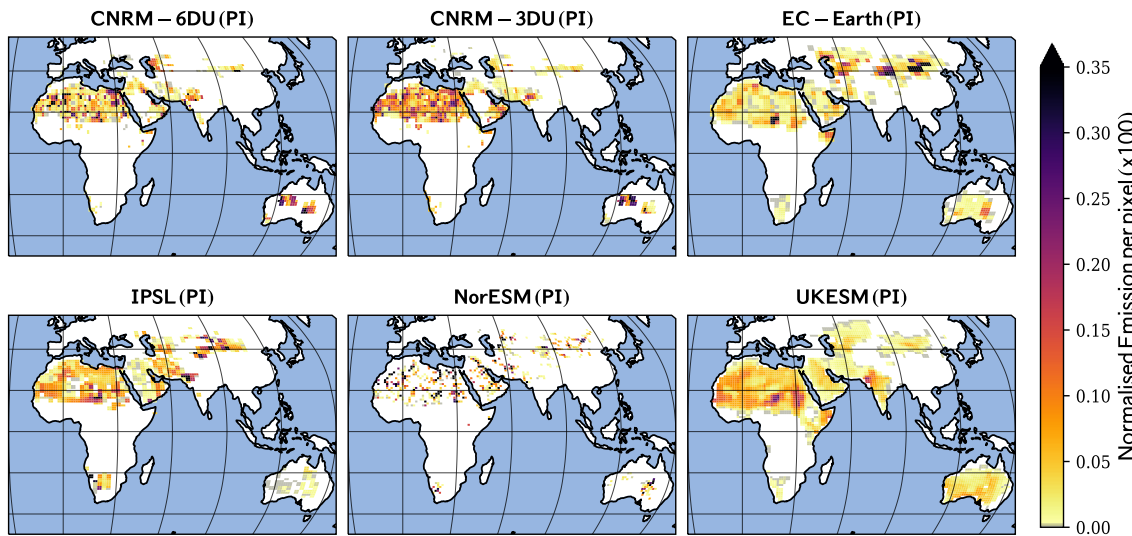


Figure S.DE.5: Normalised map of emissions (x100) over NorESM grid resolution. Experiment with pre-industrial aerosol and chemistry forcings (PI). We used a conservative near-neighbour interpolation to create emission maps that preserve global values on higher resolutions, then the maps were normalised to have a common comparison scale. The color-bar represents the normalised emission tendencies per grid with range [0,100]

References of Supplement Dust Emission (DE)

- [1] Amato T. Evan, Stephanie Fiedler, Chun Zhao, Laurent Menut, Kerstin Schepanski, Cyrille Flamant, and Owen Doherty. “Derivation of an observation-based map of North African dust emission”. In: *Aeolian Research* 16 (2015), pp. 153–162. ISSN: 1875-9637. DOI: <https://doi.org/10.1016/j.aeolia.2015.01.001>. URL: <http://www.sciencedirect.com/science/article/pii/S187596371500004X>.

DD: Dust Deposition supplement

This supplement includes additional information for the sections 4.4 main paper *Evaluation of natural aerosols in CRESCENDO-ESMs: Mineral Dust.*

Dust Deposition: additional tables

This section complements the **Table 6** and **Table 7** of the main manuscript with the equivalent tables for PDN and PI experiments.

Table S.DD.1 Equivalent of Table 6 (wet deposition) of main paper for PI experiment.

Table S.DD.2 Equivalent of Table 6 (wet deposition) of main paper for PDN experiment.

Table S.DD.3 Equivalent of Table 7 (dry deposition) of main paper for PI experiment.

Table S.DD.4 Equivalent of Table 7 (dry deposition) of main paper for PDN experiment.

Dust Wet Deposition: seasonal cycle

This section show the analogous **Figure 10** of main manuscript about the Dust Optical Depth but for *Wet deposition*. It is shown for PD, PI and PDN experiments with and without normalization.

Fig. S.DD.5 Seasonal cycle Wet-Deposition for PD experiment.

Fig. S.DD.6 Seasonal cycle Wet-Deposition for PI experiment.

Fig. S.DD.7 Seasonal cycle Wet-Deposition for PDN experiment.

Fig. S.DD.8 Seasonal cycle Wet-Deposition (not normalized) (PD experiment).

Fig. S.DD.9 Seasonal cycle Wet-Deposition (not normalized) (PI experiment).

Fig. S.DD.10 Seasonal cycle Wet-Deposition (not normalized) (PDN experiment).

Dust Deposition: Network of Instruments

This section complements the **Figure 8**, **Figure 9** and **Table 8** of the main manuscript with the equivalent figures for PDN

Fig. S.DD.11 Scatterplot total deposition flux PDN experiment [1].

Fig. S.DD.12 Scatterplot total deposition flux PDN experiment (SET-M).

Table. S.DD.13 Statistics for the PD, PDN and PI comparision with total dust deposition.

Dust Deposition: additional tables

Table S.DD.1: Total wet depositions [$Tg\ yr^{-1}$] for PI simulations. Over oceanic-regions. In brackets the order of contributions by region.

	CNRM-6DU (PI)	CNRM-3DU (PI)	EC-Earth (PI)	IPSL (PI)	NorESM (PI)	UKESM (PI)
Global Earth	2319.1	781.0	511.6	961	287.4	938
Land	1566.2	559.6	286.1	580.1	216.5	662.7
Ocean	752.9	221.4	225.5	380.9	70.9	275.2
North Atlantic	225.9 (1)	66.1 (1)	55.8 (2)	162.7 (1)	24.6 (1)	105.3 (1)
South Atlantic	11.5 (5)	5.0 (5)	14.2 (5)	45.3 (2)	2.7 (4)	13.1 (4)
North-Indian Ocean	193.5 (2)	48.2 (2)	17.6 (4)	38.0 (3)	14.8 (2)	33.8 (3)
South-Indian Ocean	40.5 (4)	13.6 (4)	4.2 (6)	12.9 (5)	2.5 (5)	12.0 (5)
Pacific East	97.1 (3)	22.0 (3)	77.0 (1)	37.2 (4)	7.0 (3)	40.5 (2)
Pacific North-West	2.0 (8)	0.3 (8)	22.5 (3)	12.4 (6)	1.0 (6)	8.5 (6)
Pacific South-West	10.0 (6)	2.7 (6)	3.1 (7)	3.6 (8)	1.0 (7)	6.1 (7)
Antarctic Ocean	5.3 (7)	2.5 (7)	2.6 (8)	6.2 (7)	0.5 (8)	4.8 (8)
Ocean North. Hemis.	604.2	170.2	193.1	292.3	58.5	211.4
Ocean South. Hemis.	148.1	51.1	32.4	87.7	12.3	63.8

Table S.DD.2: Total wet depositions [$Tg\ yr^{-1}$] for PDN simulations. Over oceanic-regions. In brackets the order of contributions by region.

	CNRM-6DU (PDN)	CNRM-3DU (PDN)	IPSL (PDN)	NorESM (PDN)
Global Earth	716.8	435.1	813.1	345.5
Land	398.6	240.4	469.9	247.9
Ocean	318.3	194.7	343.2	97.6
North Atlantic	103.7 (1)	77.6 (1)	139.5 (1)	26.6 (2)
South Atlantic	4.6 (6)	4.3 (5)	27.1 (3)	2.2 (5)
North-Indian Ocean	73 (2)	37.1 (2)	55.5 (2)	29.2 (1)
South-Indian Ocean	17 (4)	13.5 (4)	14.2 (5)	2.7 (4)
Pacific East	34.2 (3)	15.8 (3)	24 (4)	10.1 (3)
Pacific North-West	3.1 (8)	0.9 (8)	7.5 (7)	1.1 (6)
Pacific South-West	7.6 (5)	3.2 (7)	2 (8)	0.9 (7)
Antarctic Ocean	4.5 (7)	3.8 (6)	9.2 (6)	0.9 (8)
Ocean North. Hemis.	258.9	150.1	266.4	82.9
Ocean South. Hemis.	59.1	44.4	76.2	14.7

Table S.DD.3: Total dry depositions [$Tg\ yr^{-1}$] for PI simulations. Over oceanic-regions. In brackets the order of contributions by region.

	CNRM-6DU (PI)	CNRM-3DU (PI)	EC-Earth (PI)	IPSL (PI)	NorESM (PI)	UKESM (PI)
Global Earth	1415.2	1728.7	633.8	592.2	1120.1	6475.6
Land	1182.7	1503.2	562.0	524.5	1012.6	6273.1
Ocean	232.5	225.5	71.8	67.7	107.4	201.7
North Atlantic	83.1 (1)	89.0 (1)	27.8 (1)	32.6 (1)	29.5 (2)	87.0 (1)
South Atlantic	1.7 (6)	5.0 (5)	2.3 (4)	5.0 (3)	2.7 (4)	2.0 (5)
North-Indian Ocean	73.5 (2)	59.5 (2)	13.3 (2)	14.1 (2)	49.6 (1)	49.1 (2)
South-Indian Ocean	16.8 (3)	16.7 (3)	1.4 (6)	0.8 (6)	0.8 (6)	9.2 (4)
Pacific East	16.0 (4)	9.8 (4)	12.2 (3)	2.2 (5)	3.7 (3)	13.3 (3)
Pacific North-West	0.2 (7)	0.3 (7)	2.0 (5)	2.7 (4)	1.0 (5)	1.2 (6)
Pacific South-West	2.8 (5)	2.8 (6)	0.4 (7)	0.5 (7)	0.6 (7)	0.6 (7)
Antarctic Ocean	0.1 (8)	0.1 (8)	0.3 (8)	0.2 (8)	0.1 (8)	0.4 (8)
Ocean North. Hemis.	191.6	182.4	65.2	59.6	100.3	173.4
Ocean South. Hemis.	40.8	43.1	6.6	8.1	7.1	28.3

Table S.DD.4: Total dry depositions [$Tg\ yr^{-1}$] for PDN simulations. Over oceanic-regions. In brackets the order of contributions by region.

	CNRM-6DU (PDN)	CNRM-3DU (PDN)	IPSL (PDN)	NorESM (PDN)
Global Earth	499.5	1290.6	484	1387.9
Land	412.8	1122.7	430.8	1234.8
Ocean	86.7	167.9	53.2	153.1
North Atlantic	27.1 (2)	67.5 (1)	23.5 (1)	30.1 (2)
South Atlantic	0.5 (6)	3.1 (5)	3.9 (3)	3.6 (4)
North-Indian Ocean	28.5 (1)	45.7 (2)	11.9 (2)	78.9 (1)
South-Indian Ocean	5.5 (3)	10.4 (3)	0.8 (6)	1 (5)
Pacific East	5.4 (4)	5.1 (4)	1.7 (4)	6.1 (3)
Pacific North-West	0.2 (7)	0.2 (7)	1.4 (5)	0.9 (6)
Pacific South-West	1.4 (5)	1.4 (6)	0.1 (8)	0.6 (7)
Antarctic Ocean	0.1 (8)	0.1 (8)	0.5 (7)	0.1 (8)
Ocean North. Hemis.	74.2	142.3	45.2	143.4
Ocean South. Hemis.	12.4	25.6	8	9.8

Dust Wet Deposition: seasonal cycle

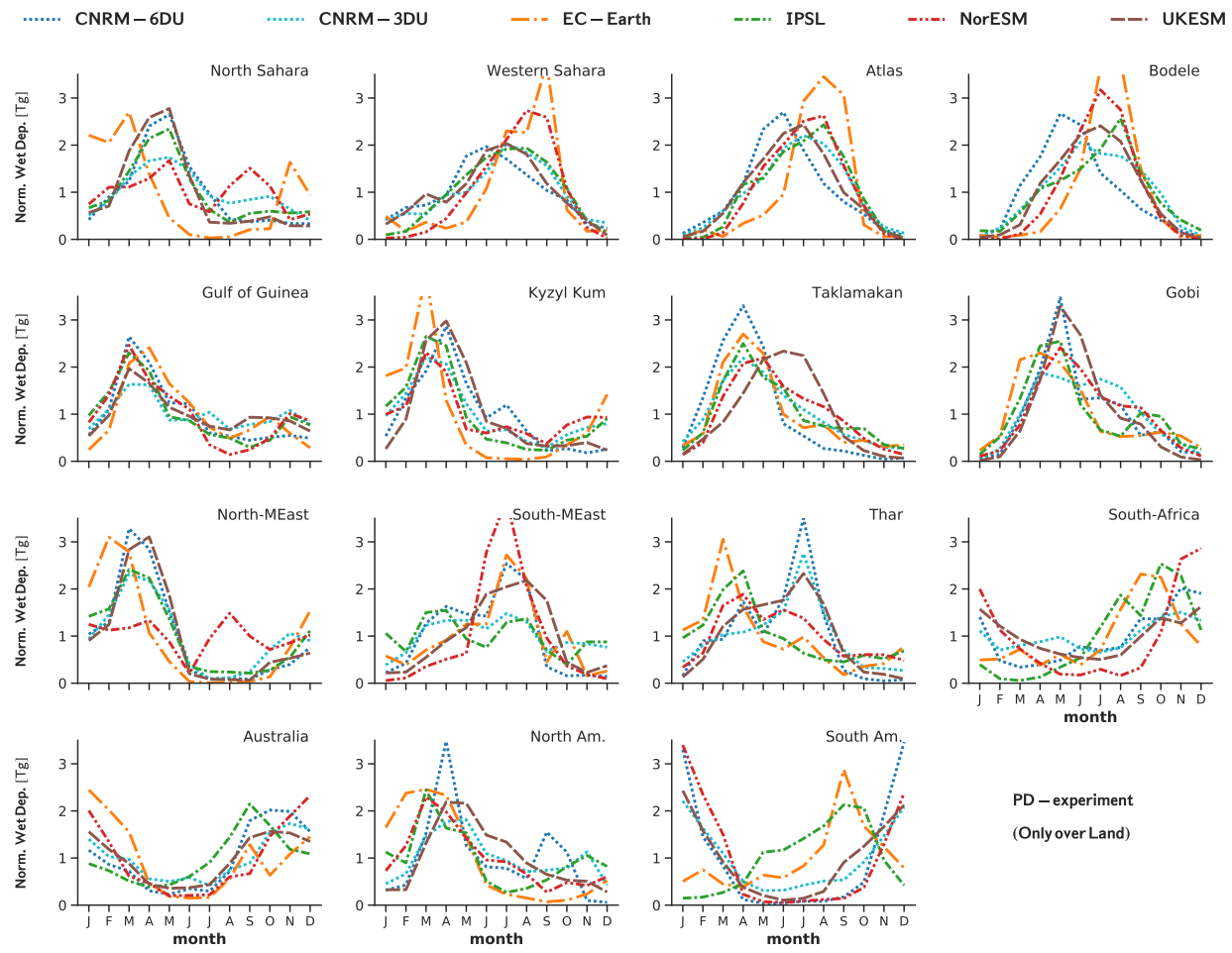


Figure S.DD.5: The seasonal cycle of Wet Deposition [$Tg\ yr^{-1}$] relative to yearly mean value as modelled by CRESCENDO-ESMs for 15 regions. PD experiment.
(Only over Land).

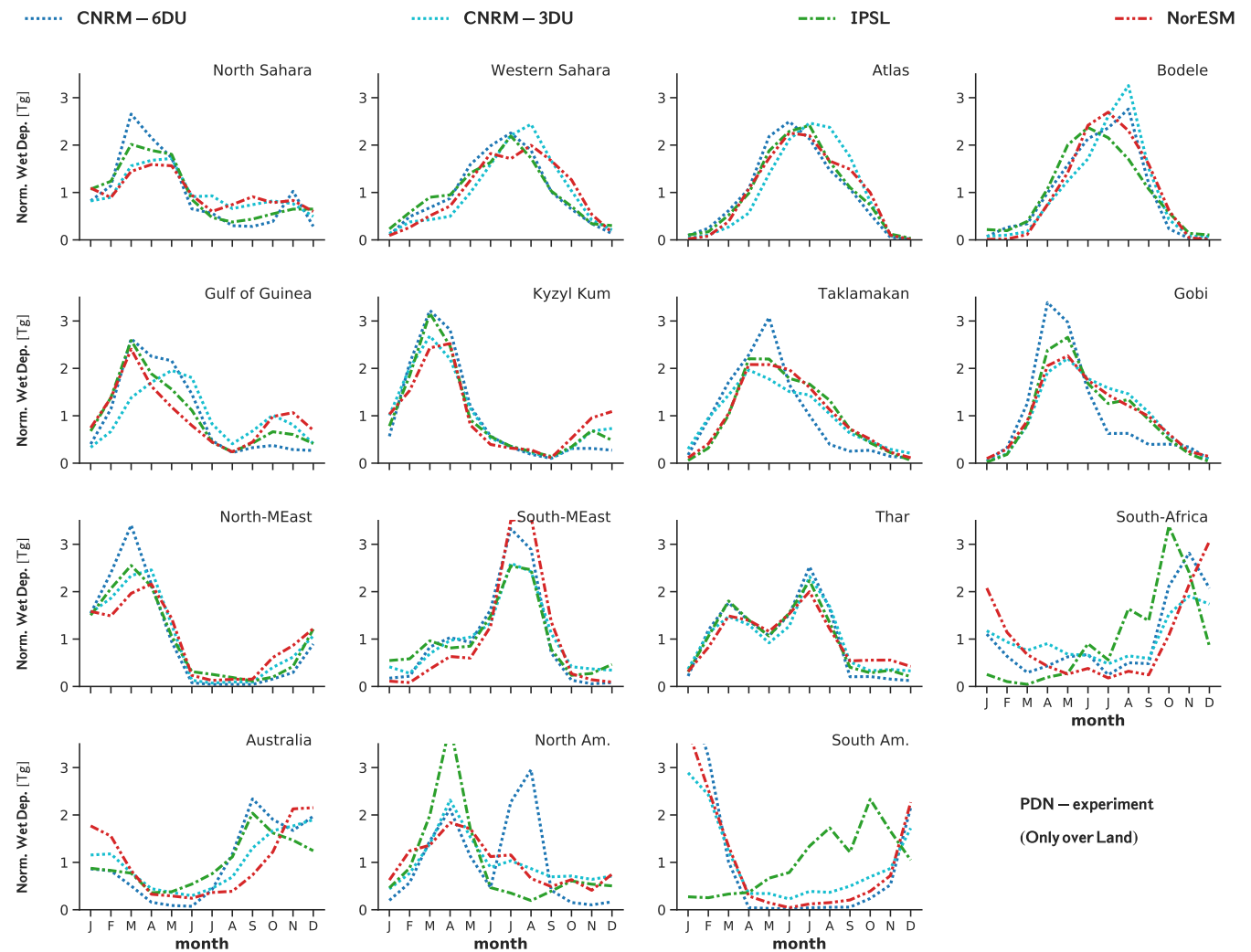


Figure S.DD.6: The seasonal cycle of Wet Deposition [$Tg\ yr^{-1}$] relative to yearly mean value as modelled by CRESCENDO-ESMs for 15 regions. PDN experiment.

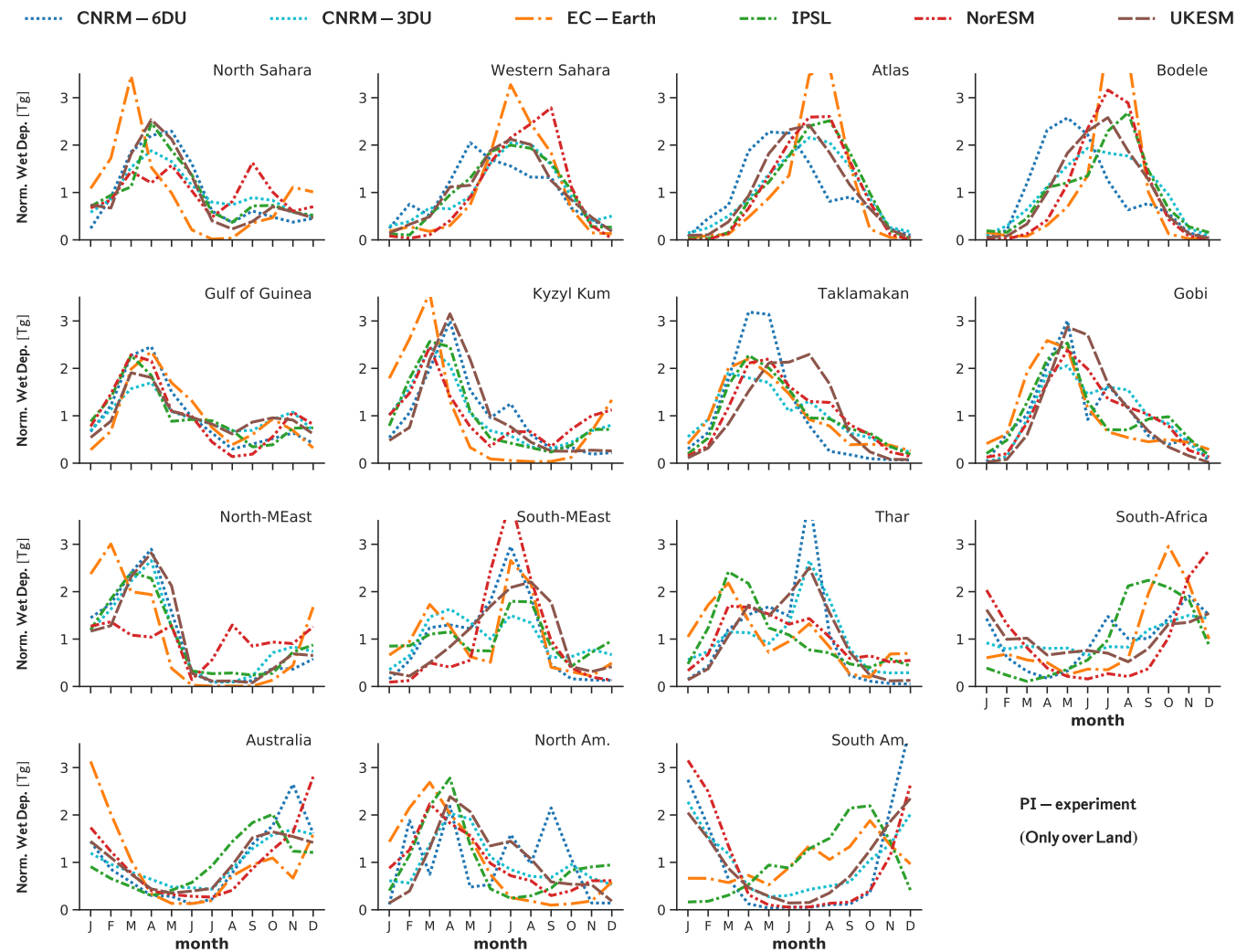


Figure S.DD.7: The seasonal cycle of Wet Deposition [$Tg\ yr^{-1}$] relative to yearly mean value as modelled by CRESCENDO-ESMs for 15 regions. PI experiment.

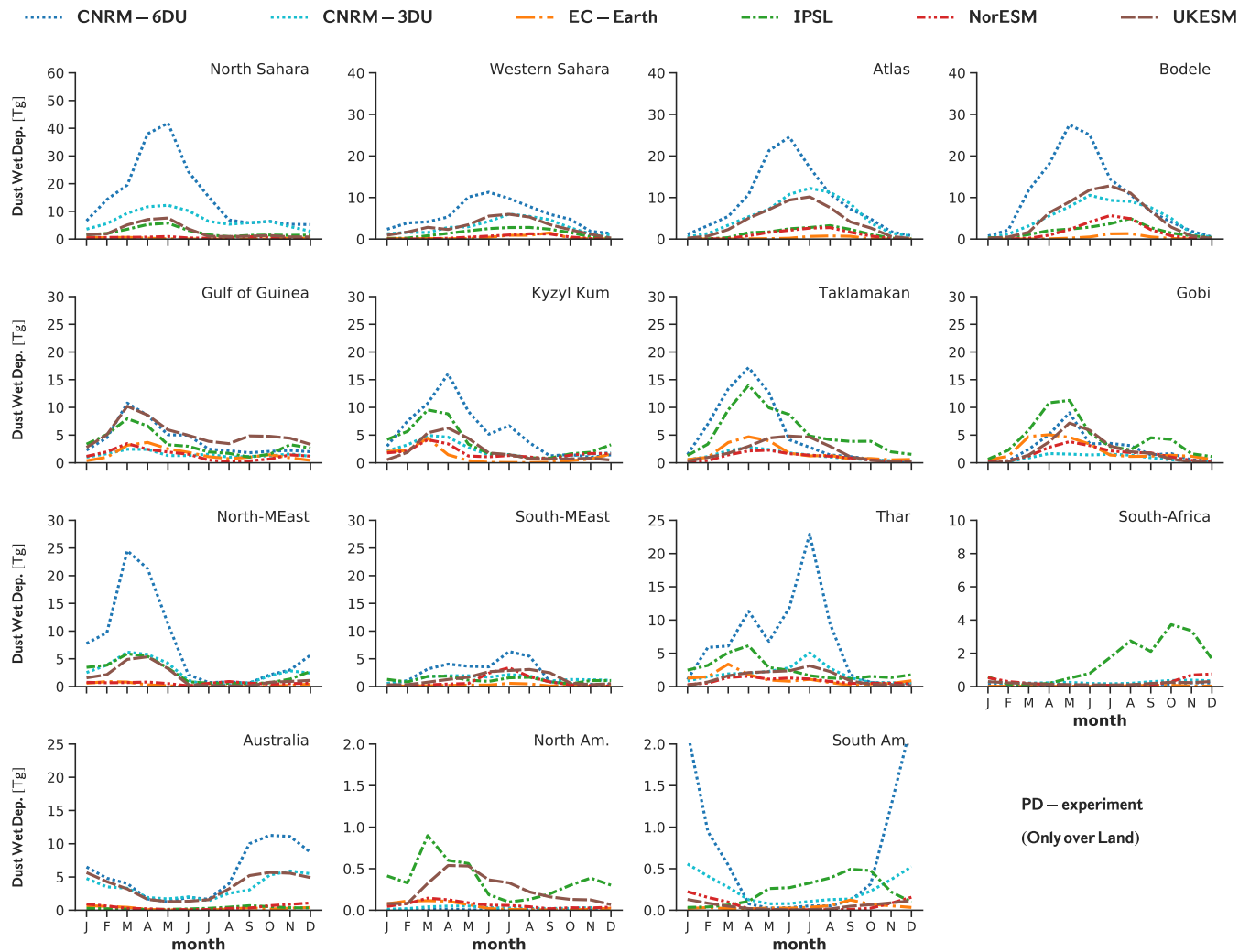


Figure S.DD.8: The seasonal cycle of Wet Deposition [$Tg\ yr^{-1}$] as modelled by CRESCENDO-ESMs for 15 regions. PD experiment.

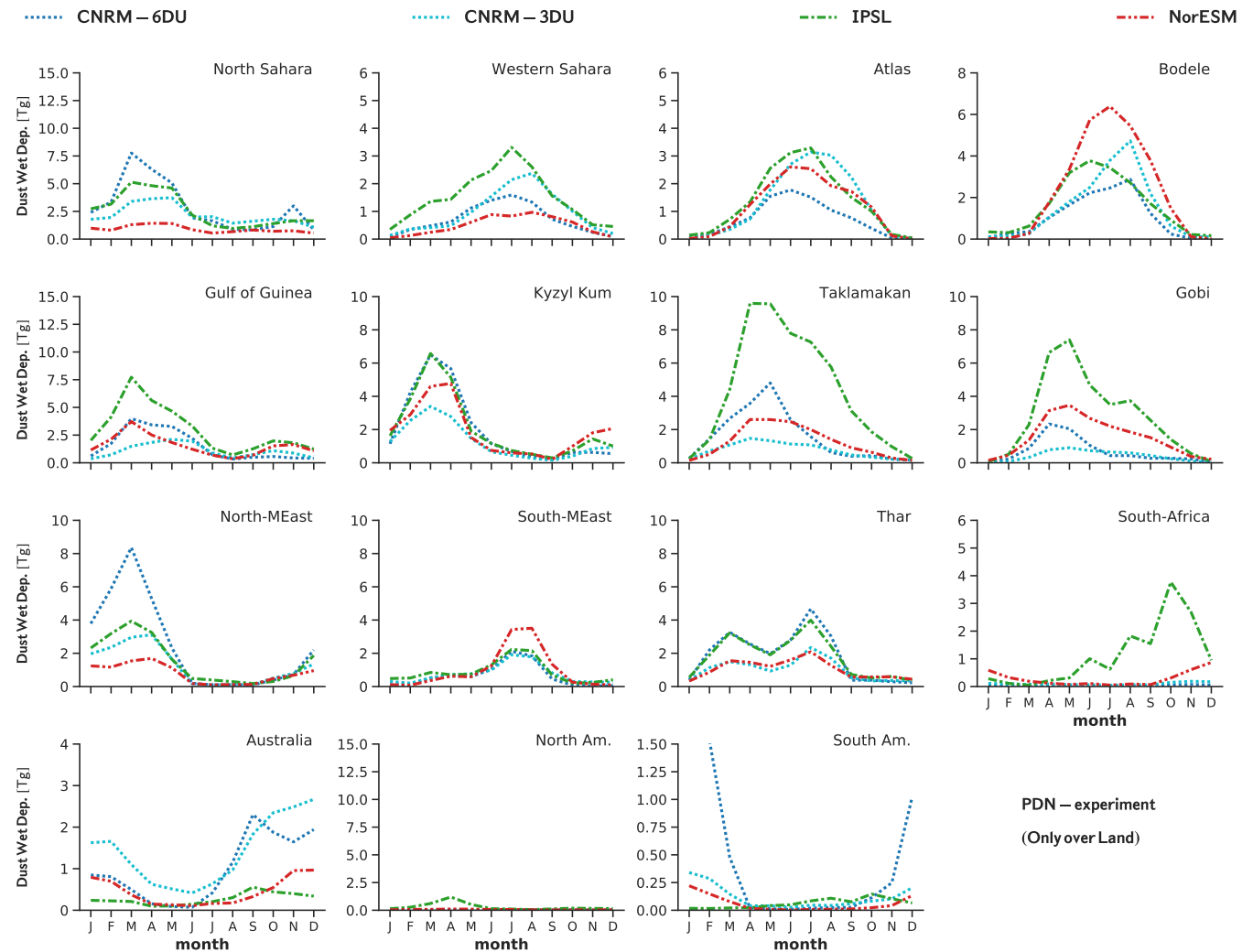


Figure S.DD.9: The seasonal cycle of Wet Deposition [$Tg\ yr^{-1}$] as modelled by CRESCENDO-ESMs for 15 regions. PDN experiment.

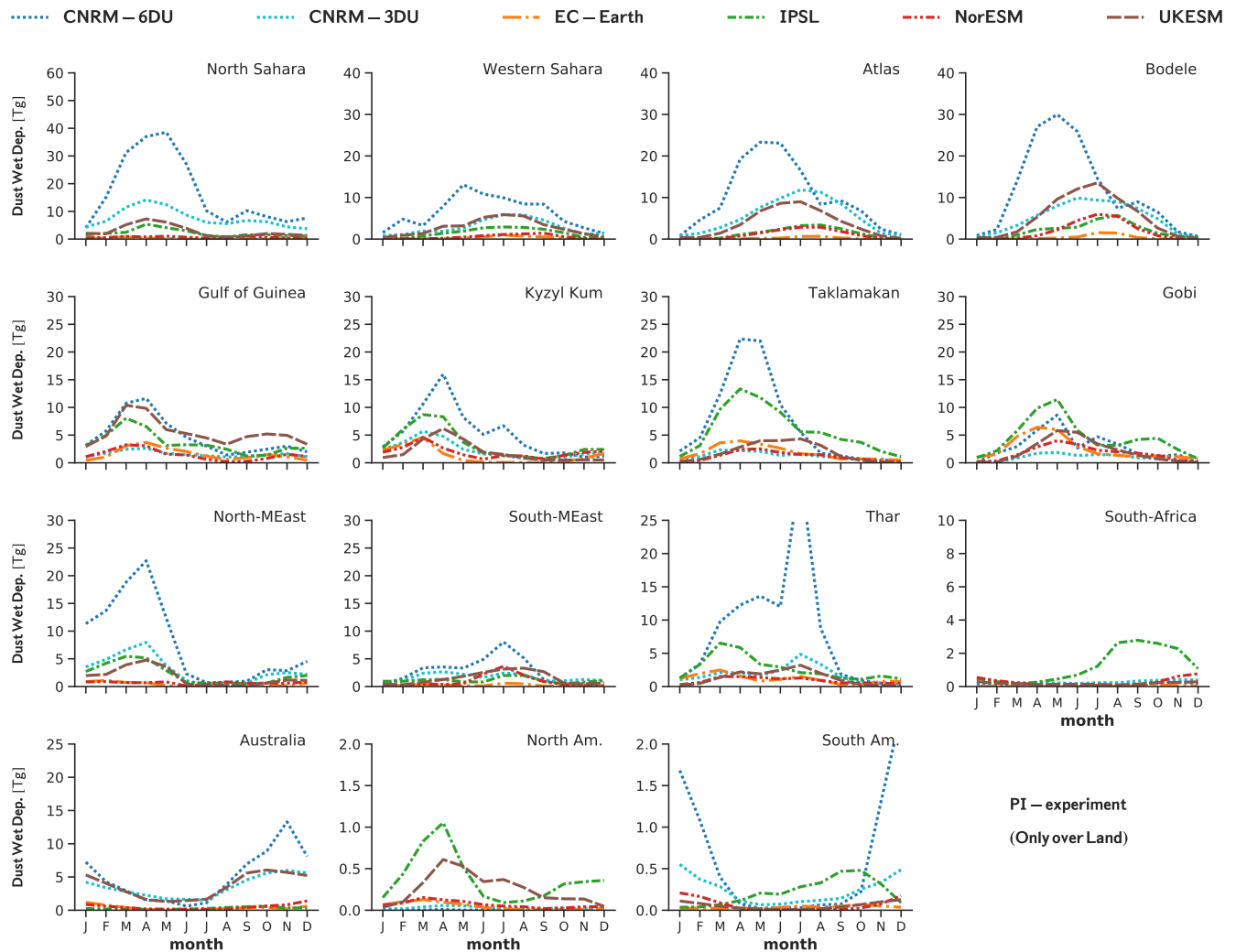


Figure S.DD.10: The seasonal cycle of Wet Deposition [$Tg\ yr^{-1}$] as modelled by CRESCENDO-ESMs for 15 regions. PI experiment.
(Only over Land)

Dust Deposition: Network of Instruments

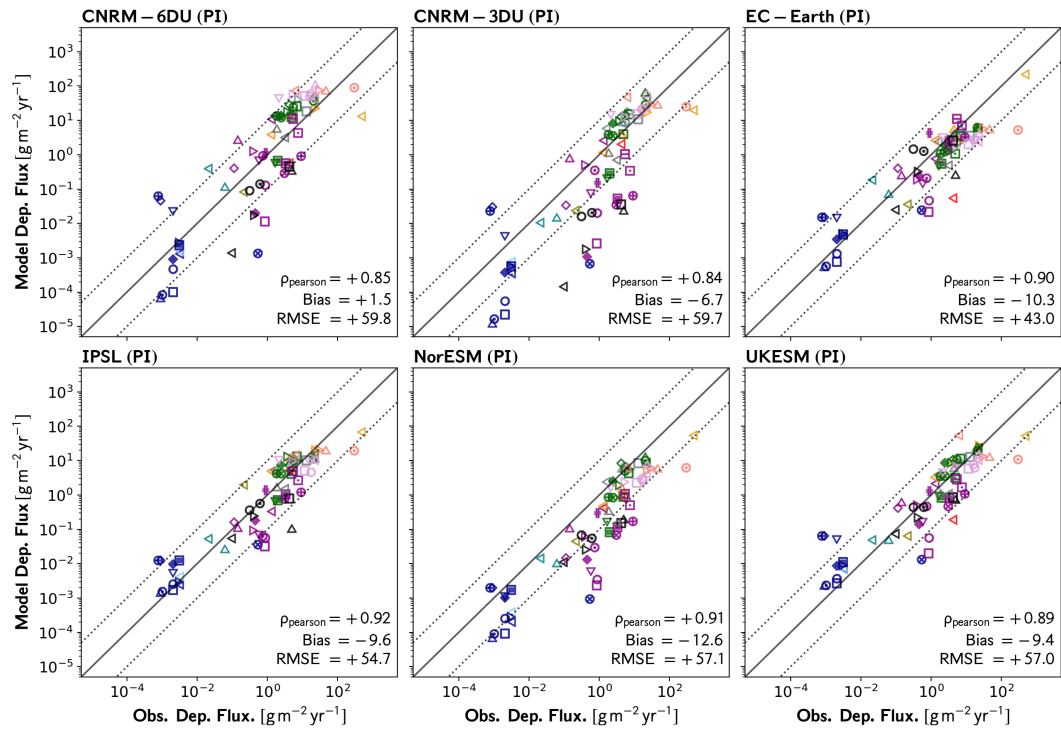


Figure S.DD.11: CRESCENDO-ESMs estimated total yearly deposition flux for PI experiment compared with the dataset presented at [1].

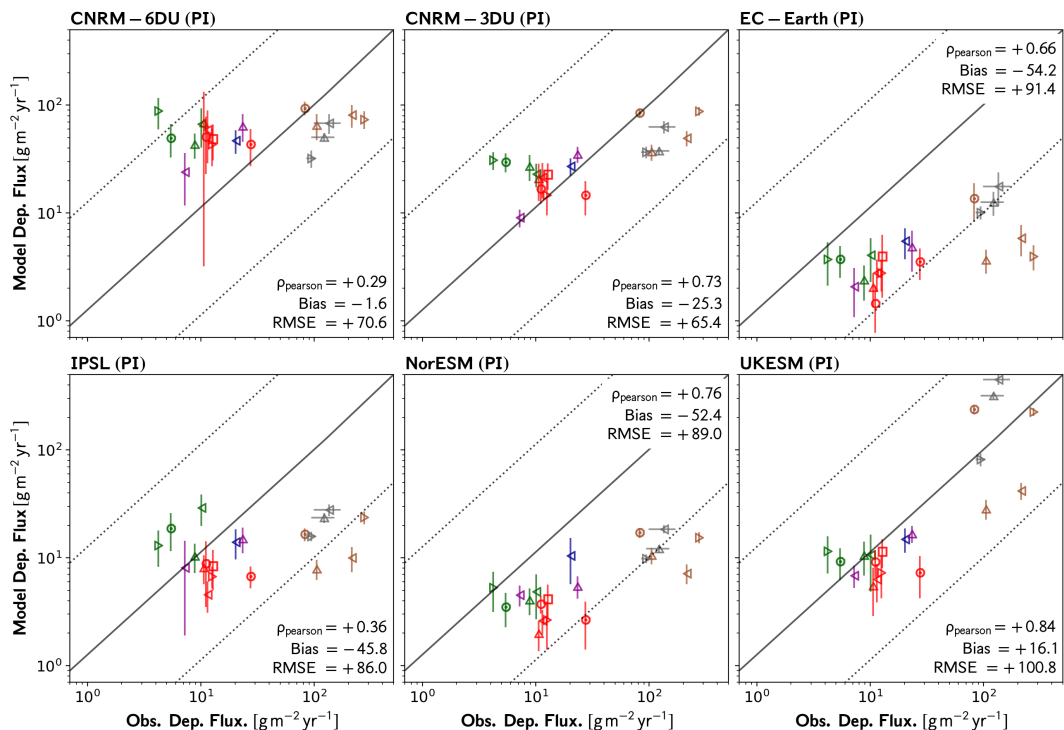


Figure S.DD.12: CRESCENDO-ESMs estimated total yearly deposition flux for PI experiment compared with the stations shown at panel (b) Figure 1 of the main paper.

Model	Exp.	Deposition Network-SET-M							Deposition Network-H2011						
		ρ	δ	δ_N	Σ	θ_N	η	ρ	δ	δ_N	Σ	θ_N	η		
CNRM-6DU	PD	+0.08	-20.18	-0.34	+0.30	+0.90	+77.75	+0.86	+0.70	+0.05	+0.41	+1.26	+60.15		
CNRM-3DU	PD	+0.34	-45.16	-0.76	+0.15	+0.85	+84.72	+0.84	-7.36	-0.48	+0.22	+0.89	+59.73		
EC-Earth	PD	+0.70	-54.12	-0.91	+0.06	+0.91	+91.26	+0.90	-10.71	-0.70	+0.36	+0.73	+45.74		
IPSL	PD	+0.51	-45.25	-0.76	+0.09	+0.83	+84.90	+0.91	-9.54	-0.62	+0.16	+0.78	+54.69		
NorESM	PD	+0.68	-52.10	-0.87	+0.07	+0.88	+89.01	+0.90	-12.68	-0.83	+0.11	+0.84	+57.26		
UKESM	PD	+0.40	-49.91	-0.84	+0.10	+0.86	+87.82	+0.89	-9.58	-0.62	+0.16	+0.81	+57.21		
CNRM-6DU	PI	+0.07	-14.00	-0.23	+0.33	+0.91	+75.08	+0.85	+1.49	+0.10	+0.41	+1.29	+59.75		
CNRM-3DU	PI	+0.25	-43.70	-0.73	+0.15	+0.83	+84.65	+0.84	-6.74	-0.44	+0.23	+0.92	+59.71		
EC-Earth	PI	+0.66	-54.17	-0.91	+0.06	+0.91	+91.39	+0.90	-10.28	-0.67	+0.42	+0.70	+43.04		
IPSL	PI	+0.36	-45.81	-0.77	+0.10	+0.84	+85.98	+0.92	-9.56	-0.62	+0.16	+0.78	+54.66		
NorESM	PI	+0.70	-51.77	-0.87	+0.07	+0.87	+88.73	+0.91	-12.58	-0.82	+0.11	+0.84	+57.12		
UKESM	PI	+0.40	-49.26	-0.83	+0.10	+0.85	+87.27	+0.75	+1.00	+0.06	+0.88	+1.69	+82.48		
CNRM-6DU	PDN	-0.08	-53.43	-0.90	+0.08	+0.92	+91.78	+0.80	-9.72	-0.63	+0.13	+0.84	+60.52		
CNRM-3DU	PDN	+0.29	-54.32	-0.91	+0.07	+0.93	+91.61	+0.78	-9.44	-0.62	+0.18	+0.88	+60.60		
IPSL	PDN	+0.51	-46.90	-0.79	+0.07	+0.84	+86.30	+0.90	-10.23	-0.67	+0.13	+0.79	+56.67		
NorESM	PDN	+0.62	-48.49	-0.81	+0.07	+0.83	+86.73	+0.89	-11.80	-0.77	+0.11	+0.83	+57.42		

Table S.DD.13: Statistical properties of the evaluation of the CRESCENDO-ESMs with respect to total dust deposition networks. Statistics metrics are described in Table 4 of main paper.

References of Supplement Dust Dep. (DD)

- [1] N. Huneeus, M. Schulz, Y. Balkanski, J. Griesfeller, J. Prospero, S. Kinne, S. Bauer, O. Boucher, M. Chin, F. Dentener, T. Diehl, R. Easter, D. Fillmore, S. Ghan, P. Ginoux, A. Grini, L. Horowitz, D. Koch, M. C. Krol, W. Landing, X. Liu, N. Mahowald, R. Miller, J.-J. Morcrette, G. Myhre, J. Penner, J. Perlitz, P. Stier, T. Takemura, and C. S. Zender. “Global dust model intercomparison in AeroCom phase I”. In: *Atmospheric Chemistry and Physics* 11.15 (2011), pp. 7781–7816. DOI: 10.5194/acp-11-7781-2011. URL: <https://www.atmos-chem-phys.net/11/7781/2011/>.

DOD: Dust Optical Depth supplement

This supplement includes additional information for the sections 4.5 main paper *Evaluation of natural aerosols in CRESCENDO-ESMs: Mineral Dust.*

Dust Optical Depth: seasonal cycle

This section complements the **Figure 10** of the main manuscript by showing the regional dust seasonal cycle for experiments different from PD, and with not normalized values.

Fig. S.DOD.1 Analogous of Figure 10 of main paper for PDN experiment.

Fig. S.DOD.2 Analogous of Figure 10 of main paper for PI experiment.

Fig. S.DOD.3 Similar to Figure 10 of main paper but without normalizing the seasonal cycle (PD experiment).

Fig. S.DOD.4 Similar to Figure 10 of main paper but without normalizing the seasonal cycle (PDN experiment).

Fig. S.DOD.5 Similar to Figure 10 of main paper but without normalizing the seasonal cycle (PI experiment).

Fig. S.DOD.6 Comparison of model-ensemble anomalies of seasonal cycle between PD and PI experiments.

Dust Optical Depth: skill dust optical depth

This section complements the **Figure 11** of the main manuscript by showing the skill with another correlation statistics (the Spearman rank correlation) for MODIS-DOD. By assuming that the time-series that the monthly time-series between models (dust optical depth at $0.55 \mu m$) and IASI (dust optical depth product at $10 \mu m$) will have similar seasonal cycle the skill of the models is ascertained against the IASI dust product (see **Figure Supp.MD.3**).

Fig. S.DOD.7 Equivalent of Figure 10 of main paper but for Spearman Correlation.

Fig. S.DOD.8 Equivalent of Figure 10 of main paper with correlations against IASI dust product (and Pearson correlation).

Fig. S.DOD.9 Equivalent of Figure 10 of main paper with correlations against IASI dust product (and Spearman correlation).

Seasonal Cycle of Aeronet Dusty Stations

Fig. S.DOD.10 Seasonal Cycle Optical Depths over Sahel Region. Models CNRM, CNRM-3DU, IPSL (PD experiment)

Fig. S.DOD.11 Seasonal Cycle Optical Depths over Sahel Region. Models NorESM and EC-Earth (PD experiment)

Dust Optical Depth: seasonal cycle

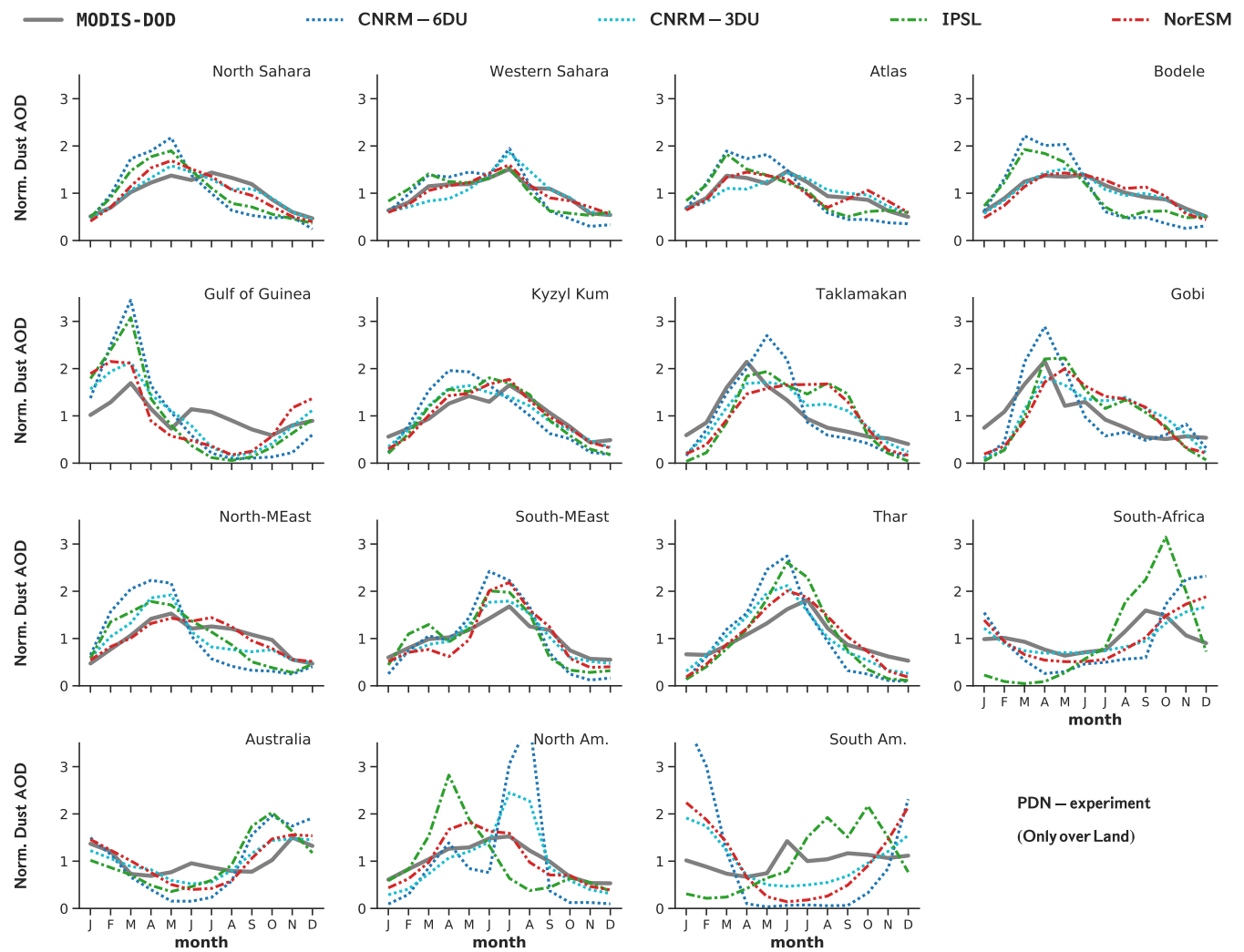


Figure S.DOD.1: The seasonal cycle of Dust Optical Depth relative to annual mean value as modelled by each CRESCENDO-ESM over 15 regions and for the PDN experiment. Compared against the DAOD product described on the supplementary information (MD) which is a derived dust optical depth over land based on MODIS deep-blue retrievals [1].

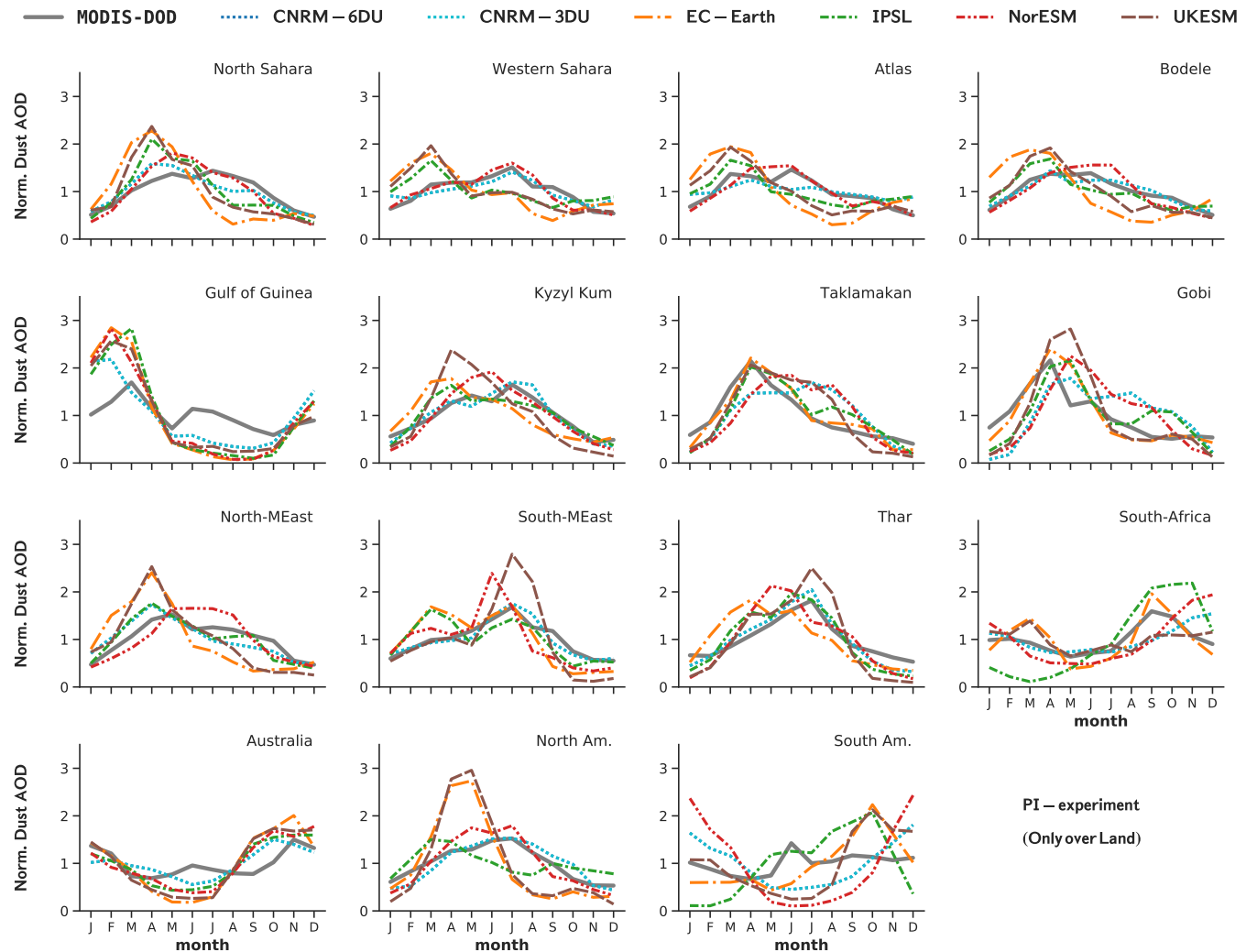


Figure S.DOD.2: The seasonal cycle of Dust Optical Depth relative to annual mean value as modelled by each CRESCENDO-ESM over 15 regions and for the PI experiment. Compared against the DAOD product described on the supplementary information (MD) which is a derived dust optical depth over land based on MODIS deep-blue retrievals [1].

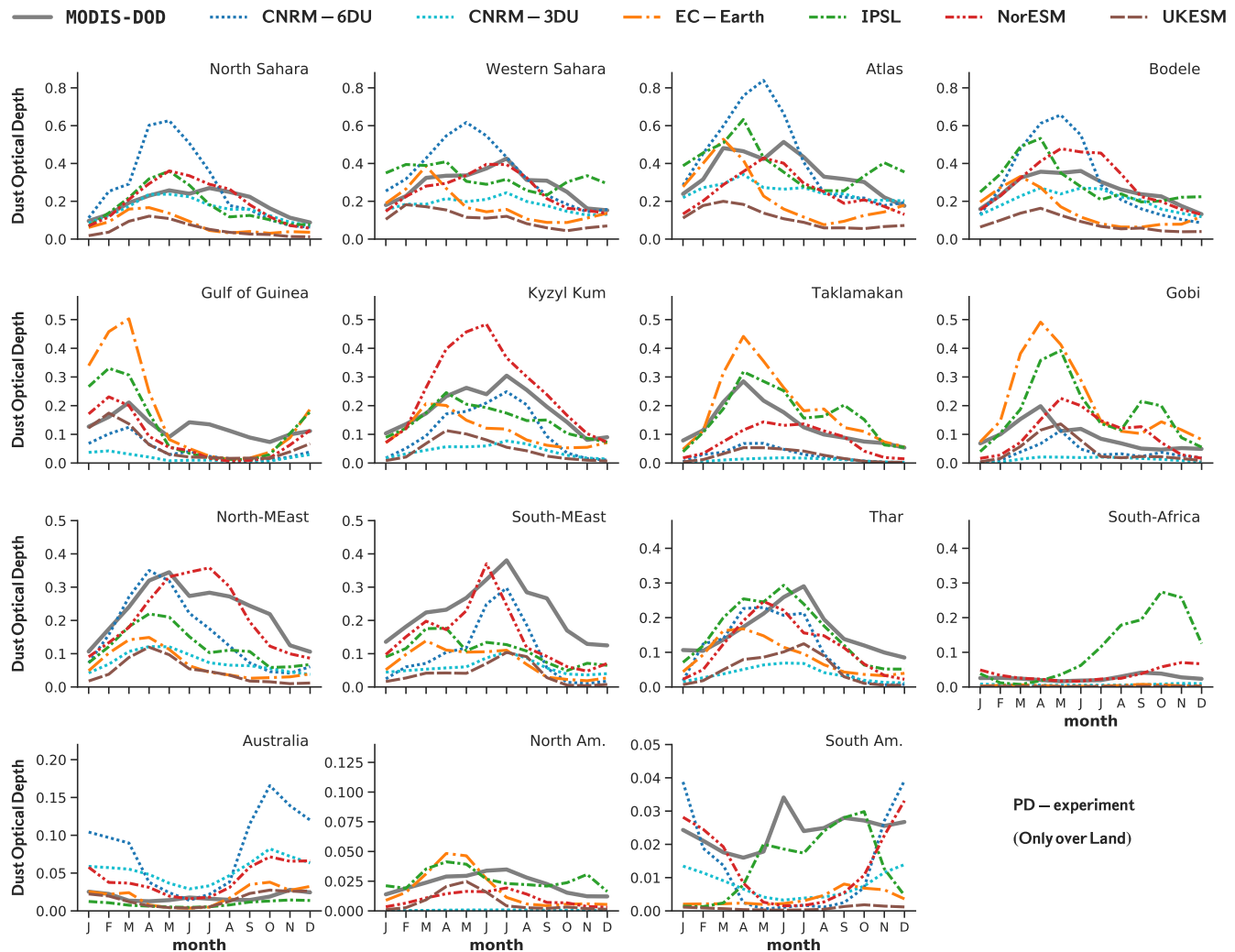


Figure S.DOD.3: The seasonal cycle of Dust Optical Depth as modelled by each CRESCENDO-ESM over 15 regions and for the PD experiment. Compared against DAOD product described on the supplementary information (MD) which is a derived dust optical depth over land based on MODIS deep-blue retrievals [1].

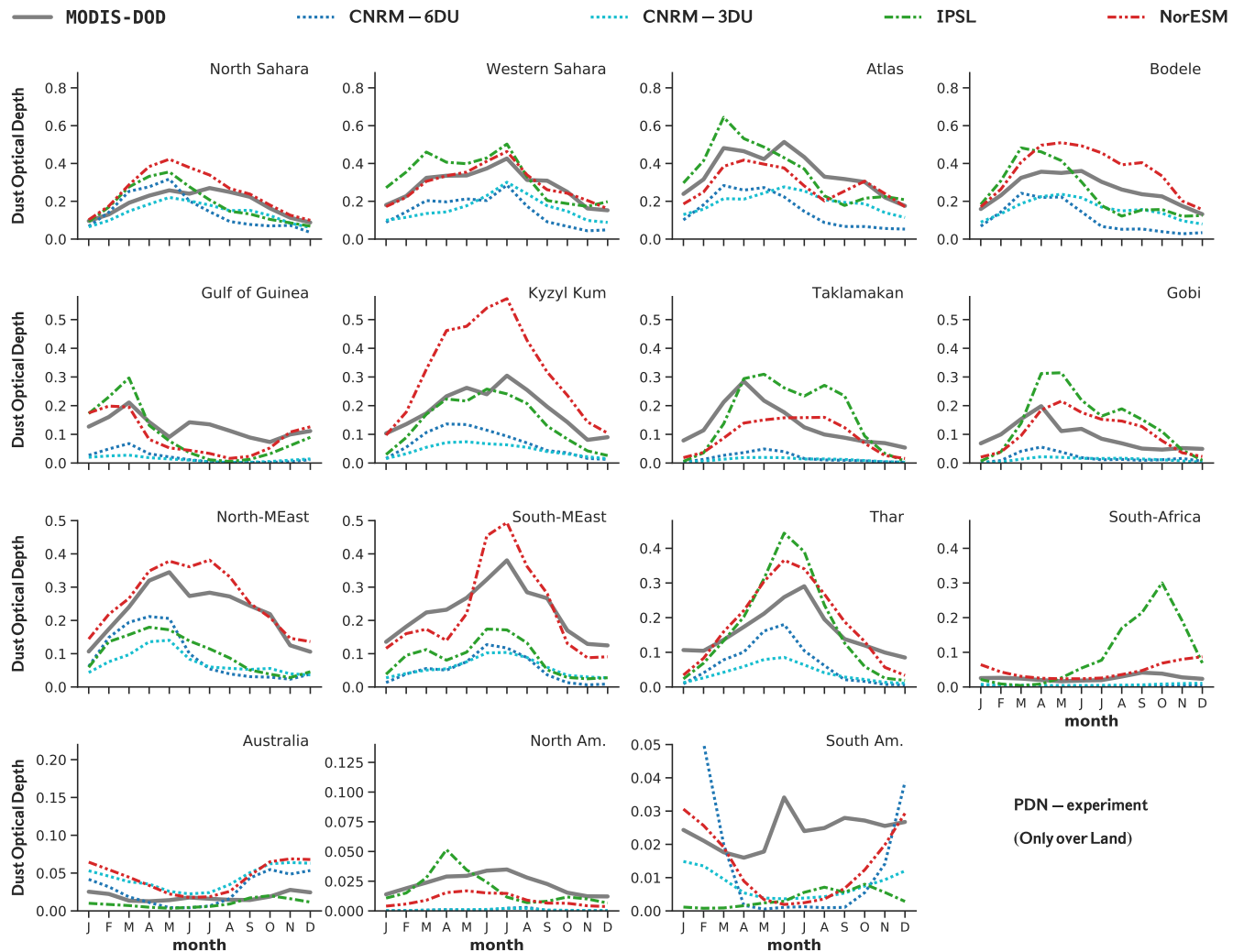


Figure S.DOD.4: The seasonal cycle of Dust Optical Depths modelled by each CRESCENDO-ESM over 15 regions and for the PDN experiment. Compared against DAOD product described on the supplementary information (MD) which is a derived dust optical depth over land based on MODIS deep-blue retrievals [1].

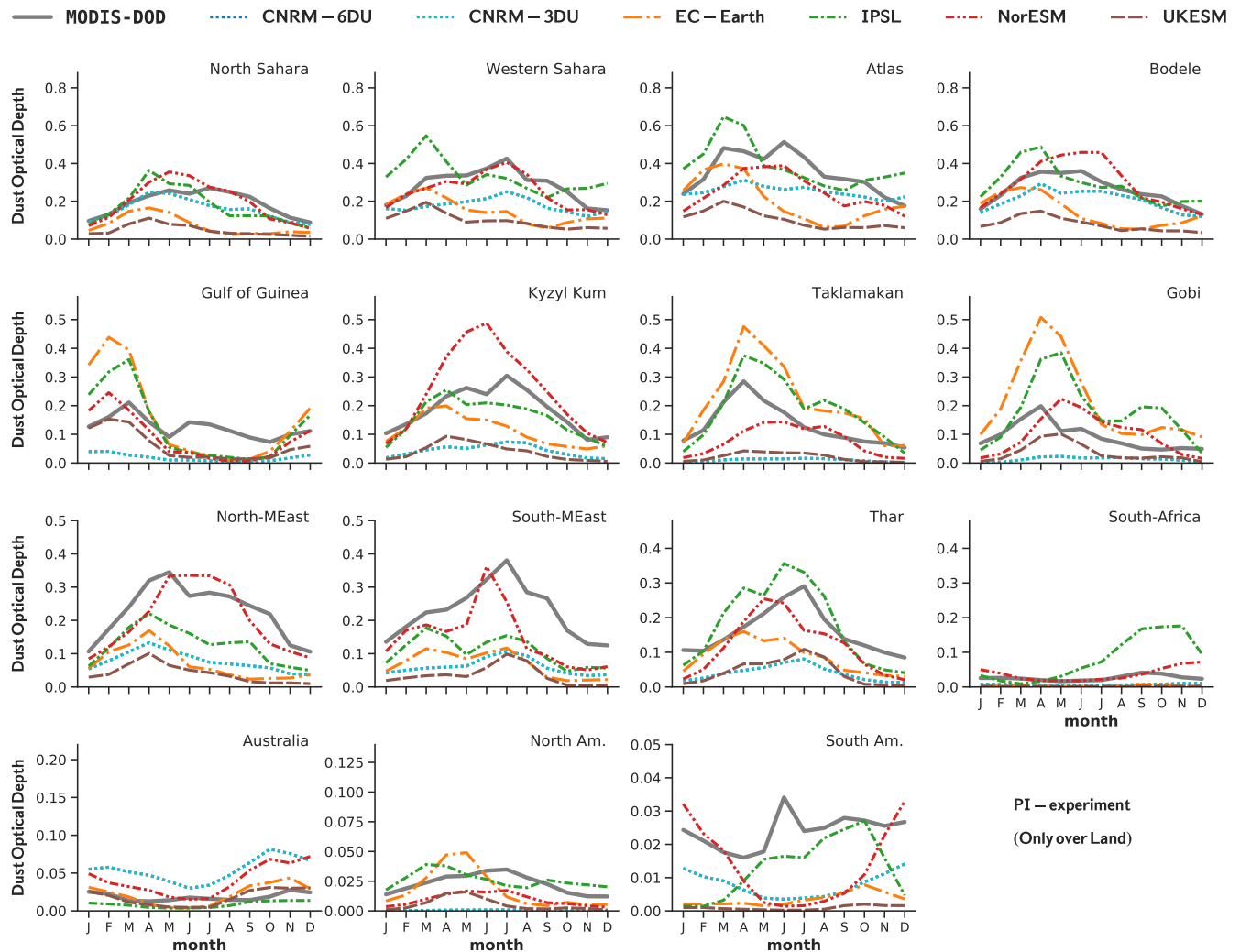


Figure S.DOD.5: The seasonal cycle of Dust Optical Depth as modelled by each CRESCENDO-ESM over 15 regions and for the PI experiment. Compared against DOD product described on the supplementary information (MD) which is a derived dust optical depth over land based on MODIS deep-blue retrievals [1].

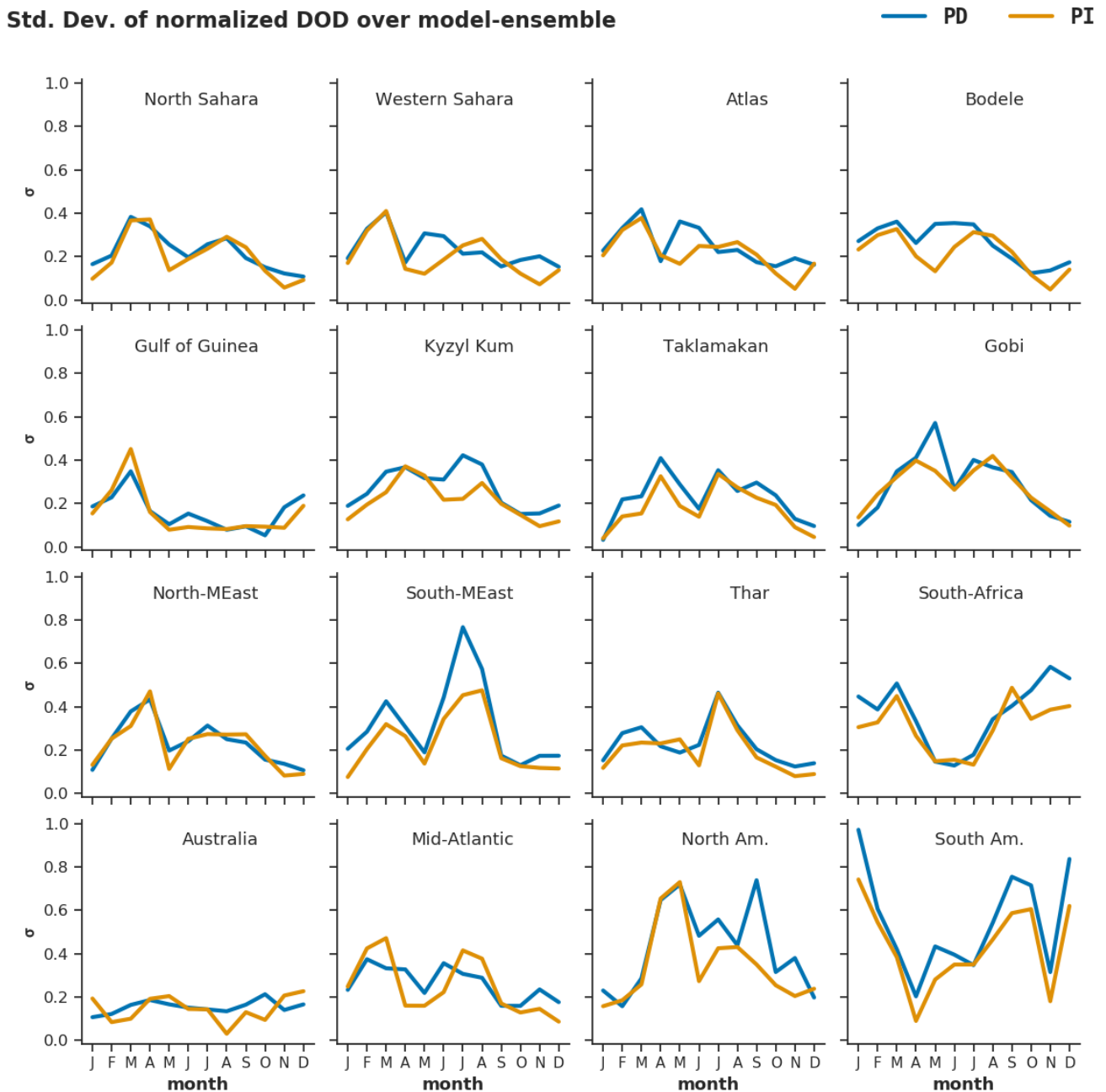


Figure S.DOD.6: Analysis of the standard deviation within the multi-model ensemble of normalized dust optical depth seasonal values. The figure compares the variability in the model-ensemble between PD and PI experiments.

Dust Optical Depth: skill dust optical depth

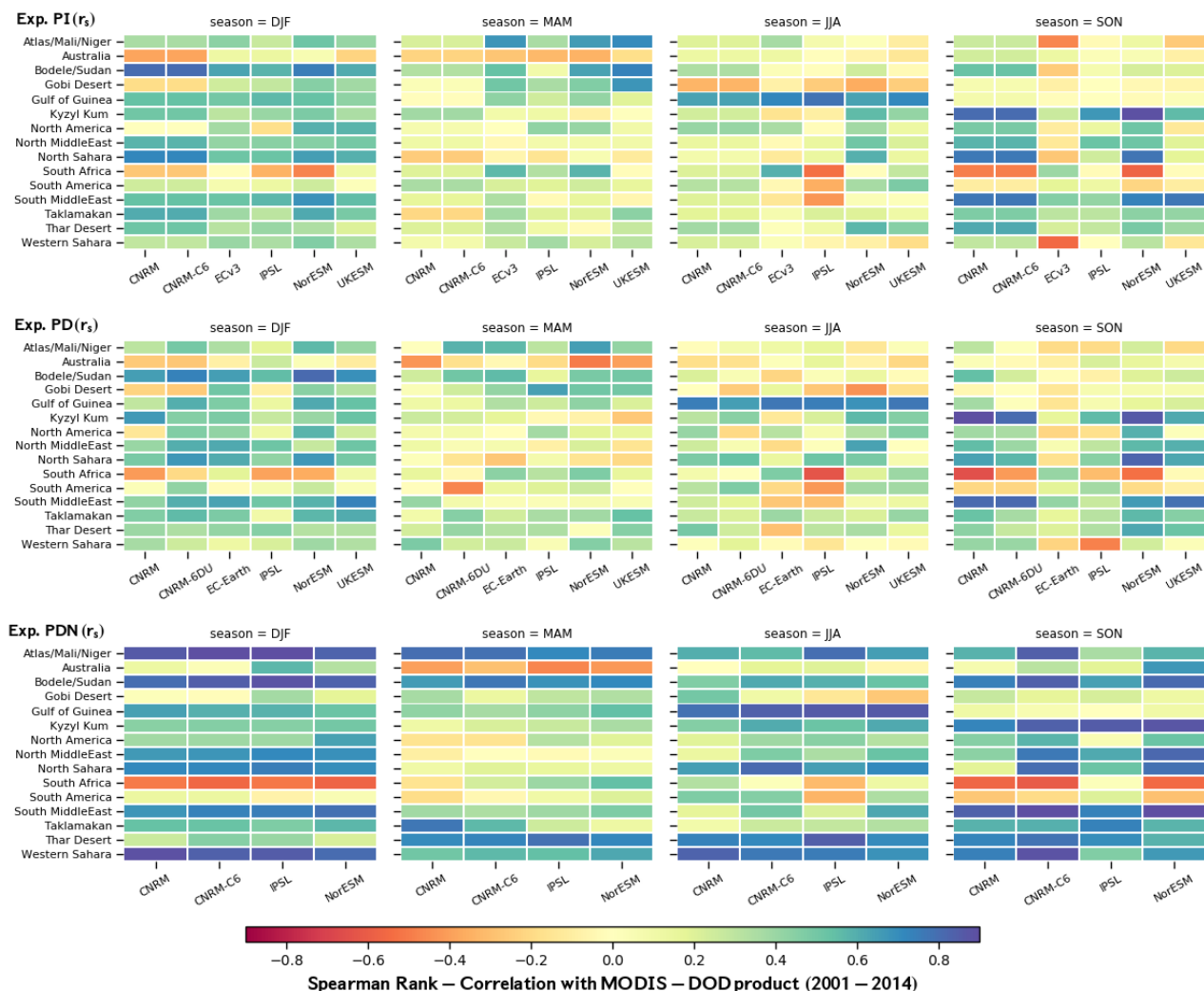


Figure S.DOD.7: Skill of CRESCENDO-ESMs for the DAOD over 15 regions and defined by the Spearman correlation between ESM time-series of dust optical depths for each season and region and that from MODIS-DOD. Time interval 2001–2014.

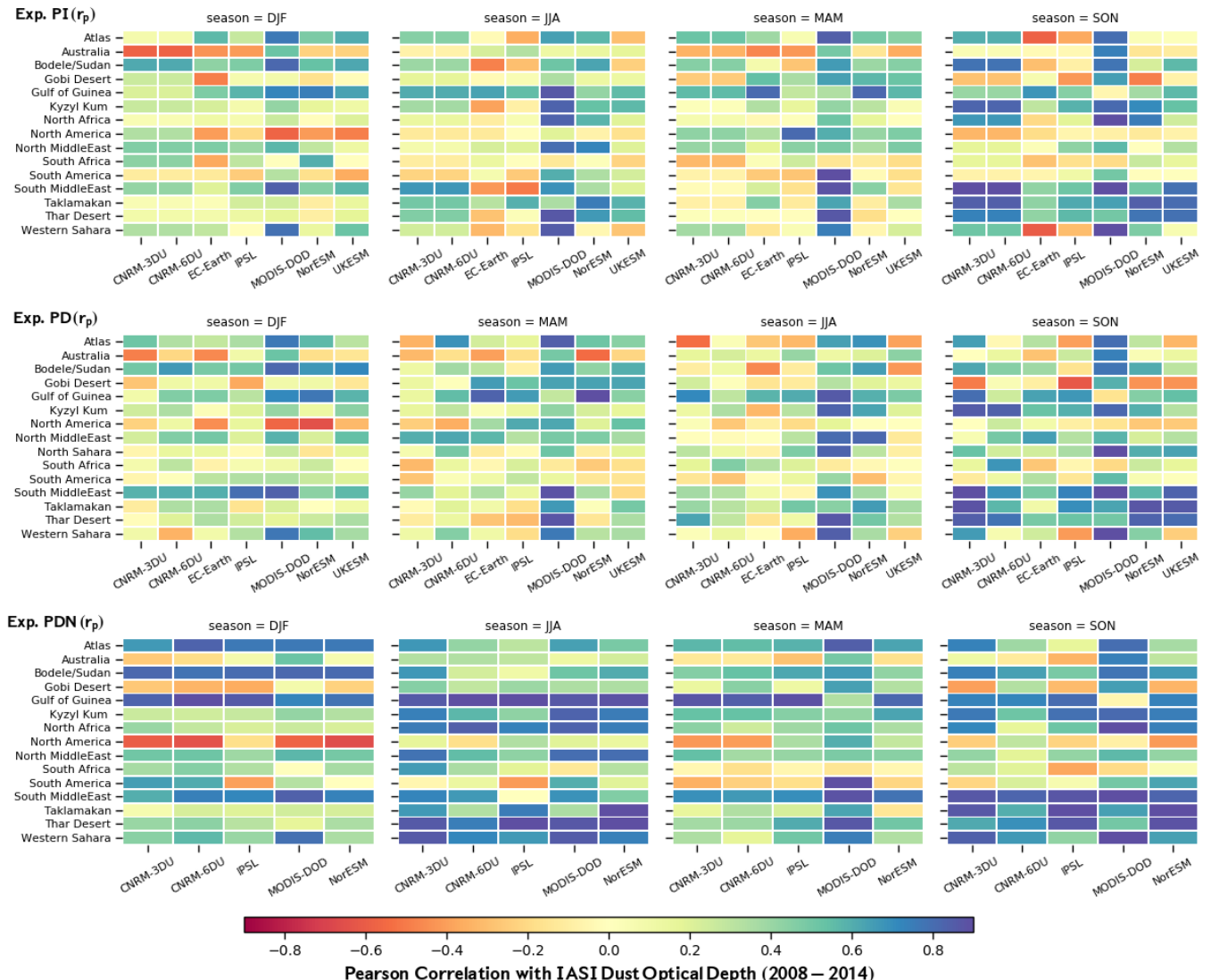


Figure S.DOD.8: Skill of CRESCENDO-ESMs for the DAOD over 15 regions and defined by the Pearson correlation between ESM time-series of dust optical depths for each season and region and that from IASI. Time interval 2008–2014.

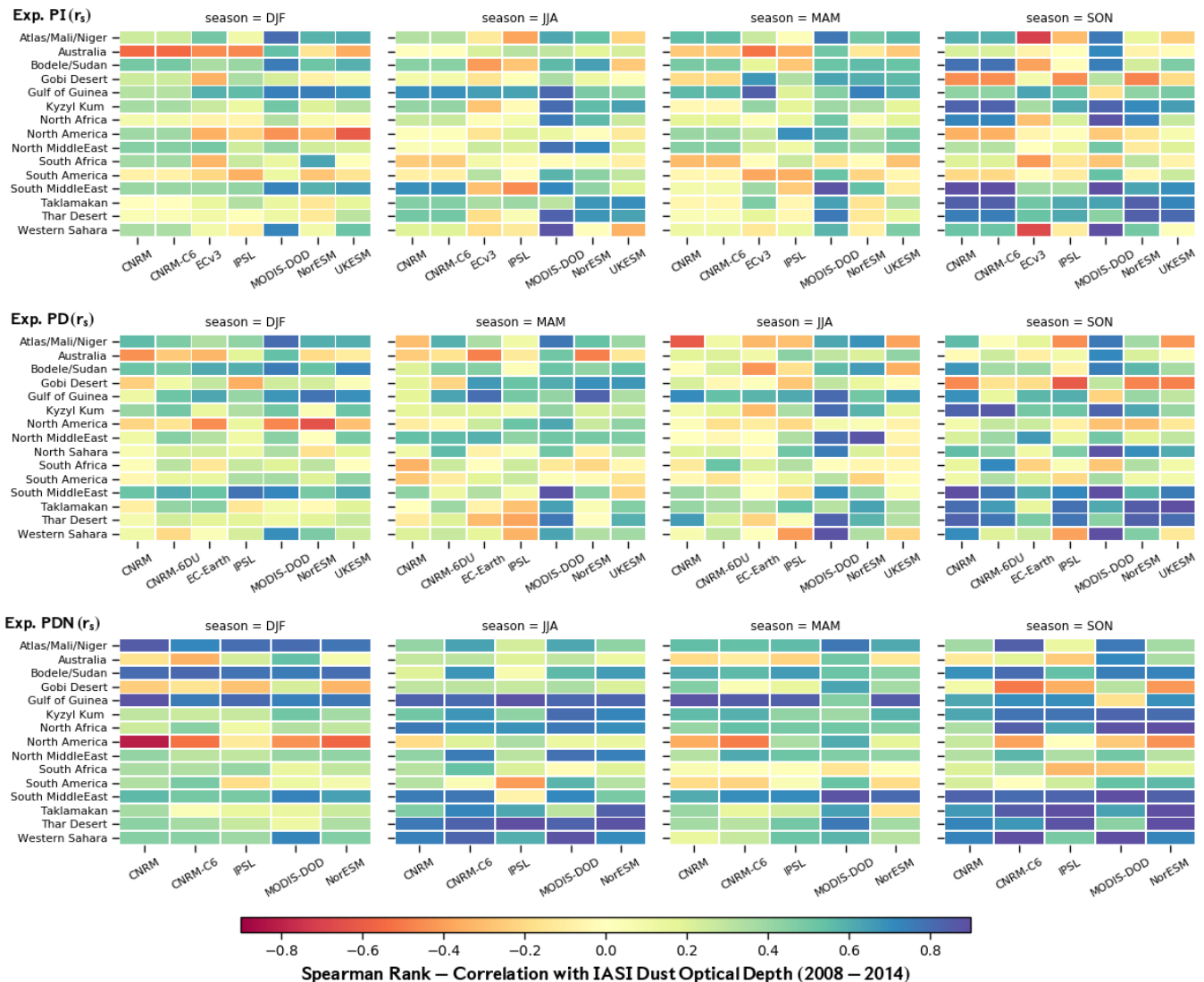


Figure S.DOD.9: Skill of CRESCENDO-ESMs for the DAOD over 15 regions and defined by the Spearman correlation between ESM time-series of dust optical depths for each season and region and that from IASI. Time interval 2008-2014.

Seasonal Cycle of AERONETv3 Stations



Figure S.DOD.10: Comparison of ESM models CNRM-6DU, CNRM-3DU and IPSL (PD simulation) against AERONETv3 stations over Sahel region.

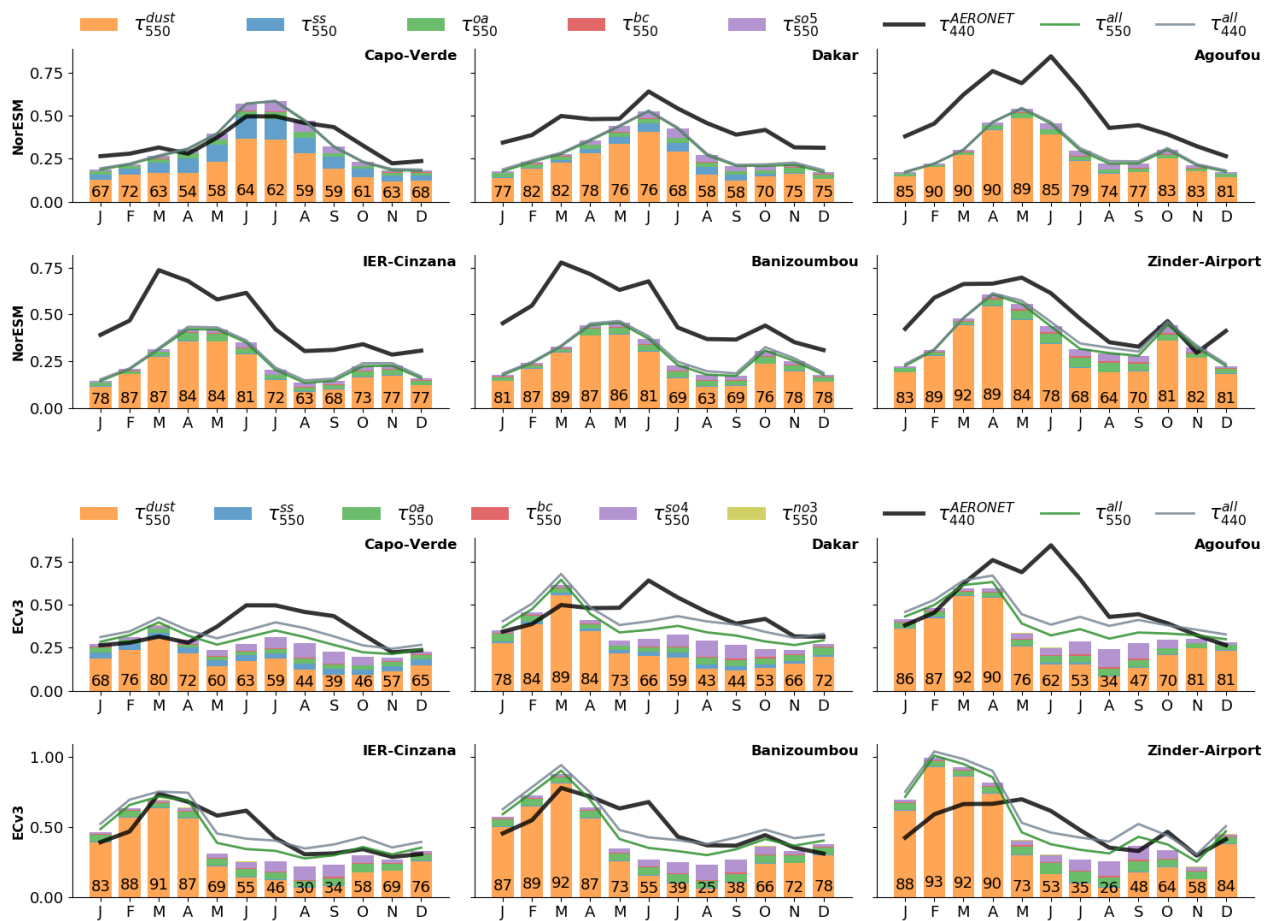


Figure S.DOD.11: Comparison of ESM models NorESM and EC-Earth (PD simulation) against AERONETv3 stations over Sahel region.

References of Supplement Dust Opt.Dep. (DOD)

- [1] B. Pu and P. Ginoux. "How reliable are CMIP5 models in simulating dust optical depth?" In: *Atmospheric Chemistry and Physics* 18.16 (2018), pp. 12491–12510. DOI: 10.5194/acp-18-12491-2018. URL: <https://www.atmos-chem-phys.net/18/12491/2018/>.

DSC: Dust Surface Concentrations supplement

This supplement includes additional information for the sections 4.6 main paper *Evaluation of natural aerosols in CRESCENDO-ESMs: Mineral Dust.*

Dust Surface Concentrations: seasonal cycle by regions

This section show the analogous **Figure 7** for surface concentrations of the main manuscript for PD, PI and PDN experiments with and without normalization.

Fig. S.DSC.1 Seasonal cycle Surface Concentrations for PD experiment.

Fig. S.DSC.2 Seasonal cycle Surface Concentrations for PDN experiment.

Fig. S.DSC.3 Seasonal cycle Surface Concentrations for PI experiment.

Fig. S.DSC.4 Seasonal cycle Surface Concentrations (not normalized) (PD experiment).

Fig. S.DSC.5 Seasonal cycle Surface Concentrations (not normalized) (PDN experiment).

Fig. S.DSC.6 Seasonal cycle Surface Concentrations (not normalized) (PI experiment).

Seasonal Cycle of Surface Concentrations: comparison with climatological dataset

Fig. S.DSC.7 Seasonal Cycle Surface Concentrations PDN experiment

Fig. S.DSC.8 Seasonal Cycle Surface Concentrations PI experiment

Network of Surface Concentrations

Table S.DSC.9 Table with statistics information of PD, PDN and PI experiments.

Fig. S.DSC.10 Seasonal Cycle Surface Concentrations PI experiment

Dust Surface Concentrations: seasonal cycle by regions

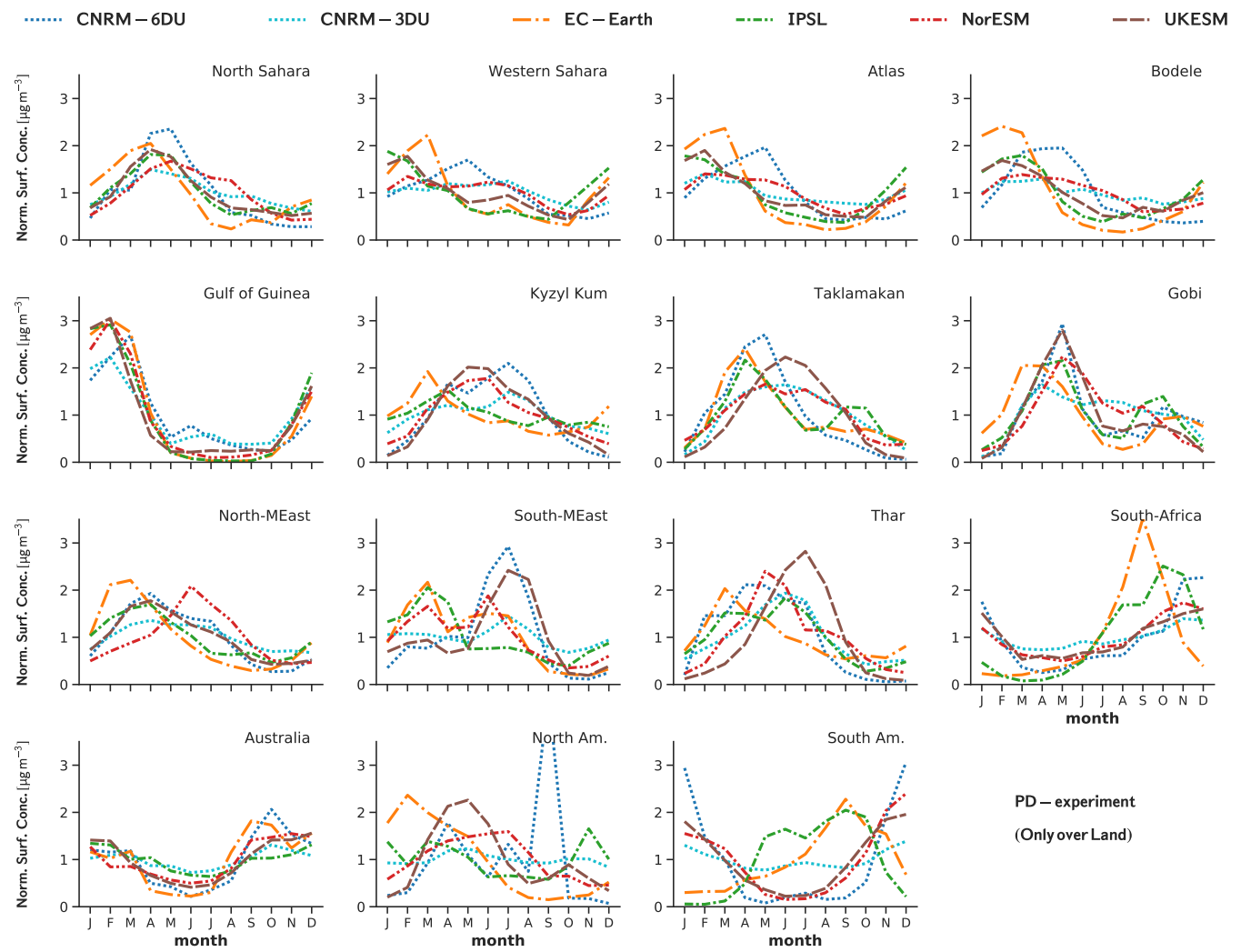


Figure S.DSC.1: The seasonal cycle of Dust surface concentration relative to yearly mean value as modelled by CRESCENDO-ESMs for 15 regions. PD experiment.

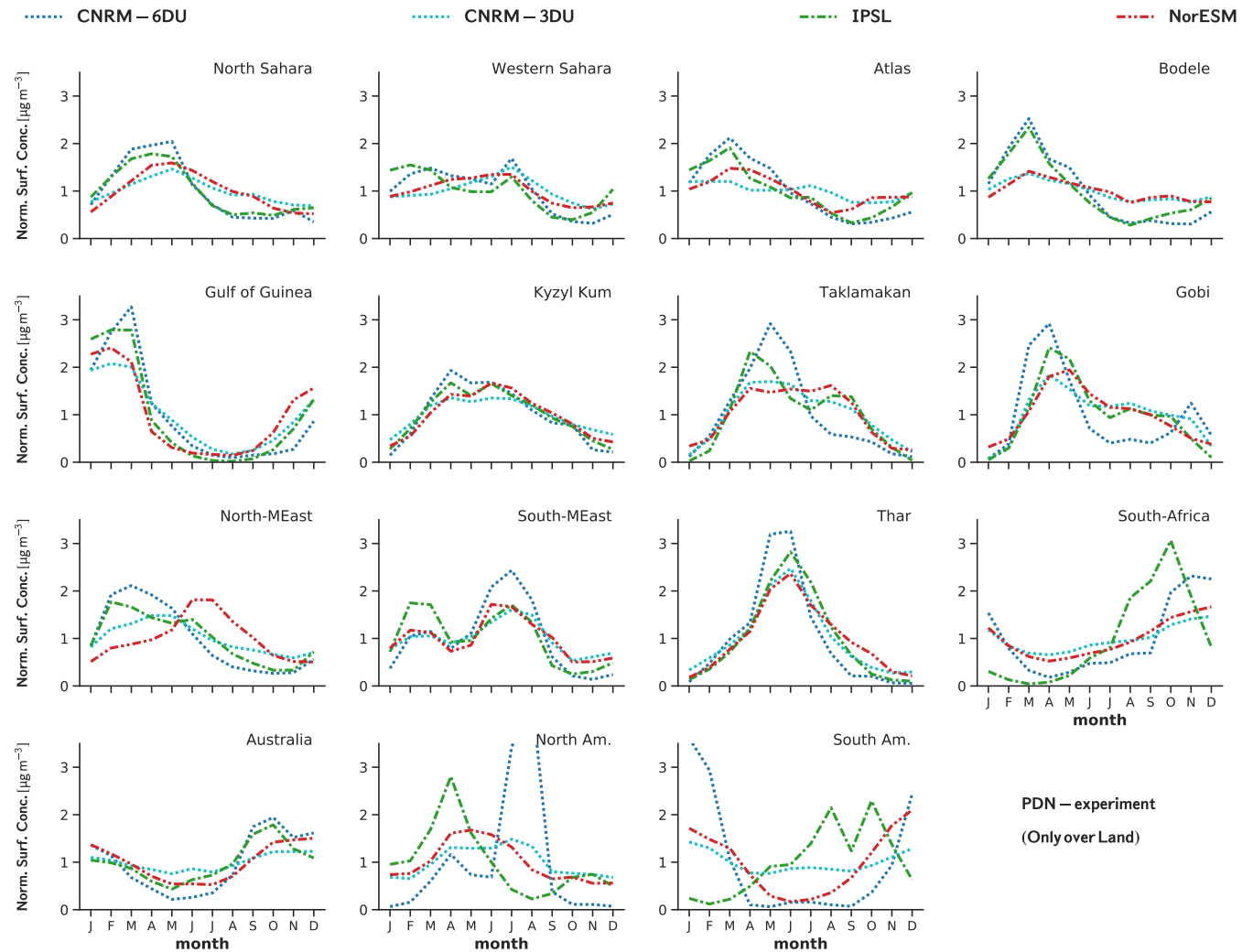


Figure S.DSC.2: The seasonal cycle of Dust surface concentration relative to yearly mean value as modelled by CRESCENDO-ESMs for 15 regions. PDN experiment.

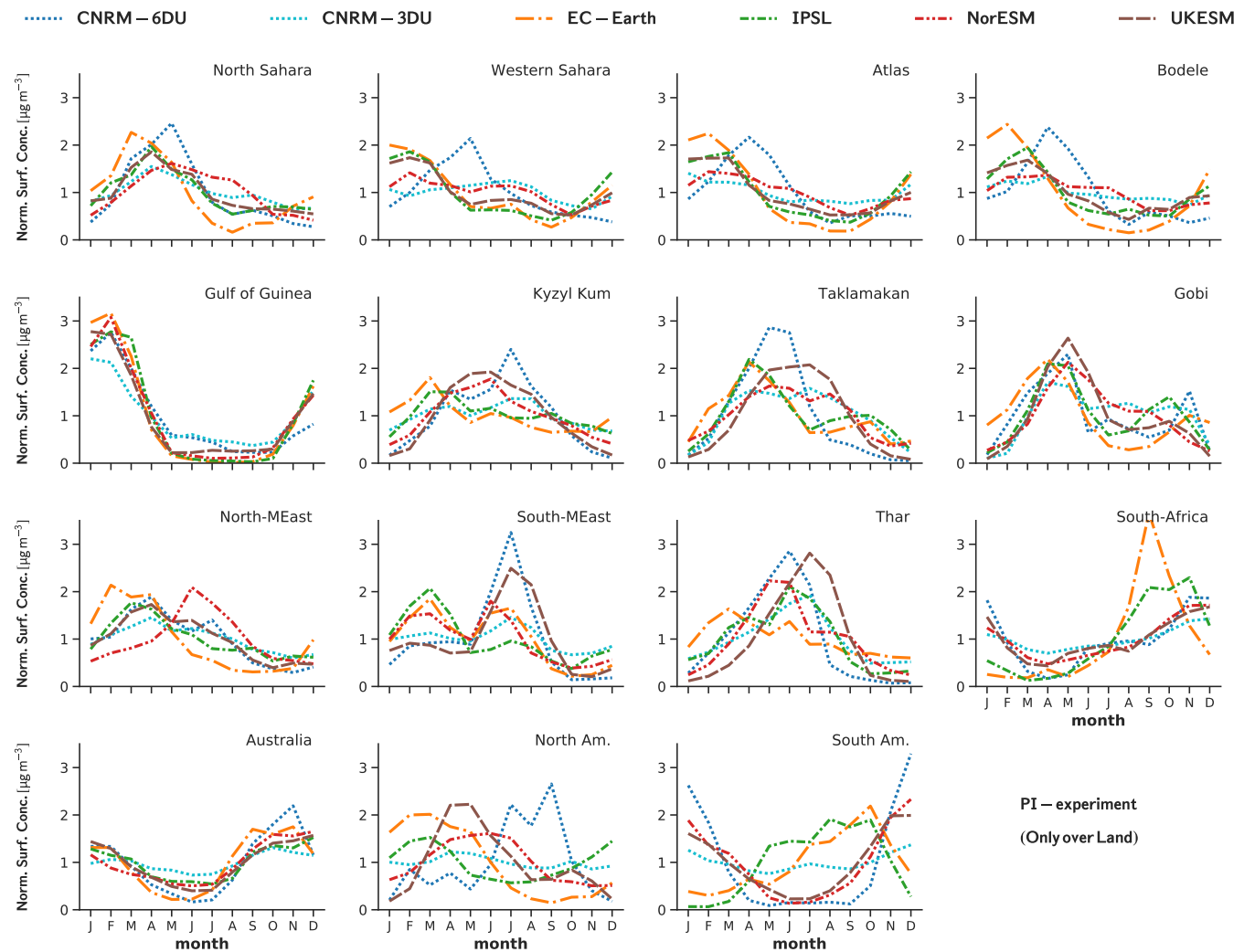


Figure S.DSC.3: The seasonal cycle of Dust surface concentration relative to yearly mean value as modelled by CRESCENDO-ESMs for 15 regions. PI experiment.

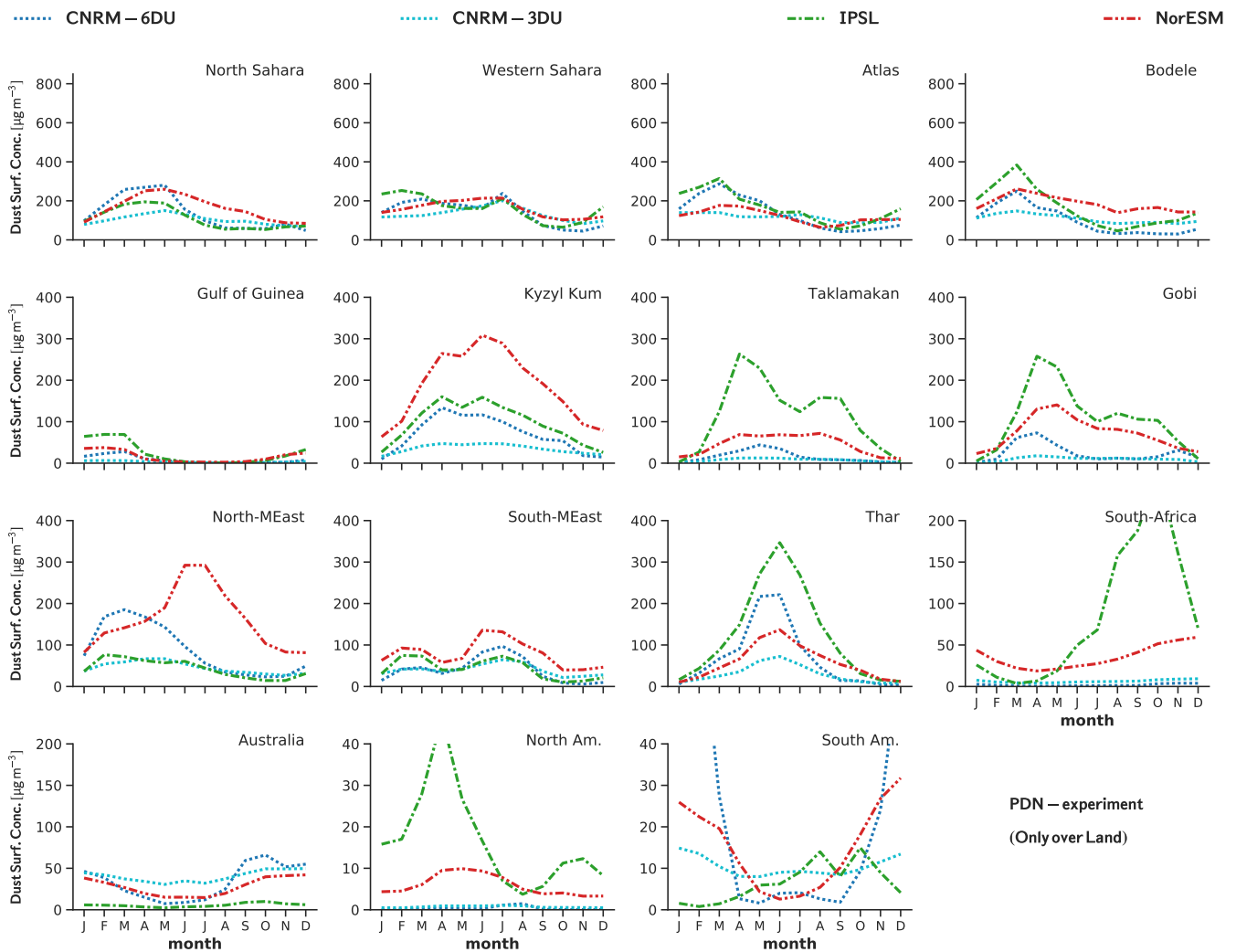


Figure S.DSC.4: The seasonal cycle of Dust surface concentration as modelled by CRESCENDO-ESMs for 15 regions. PDN experiment.

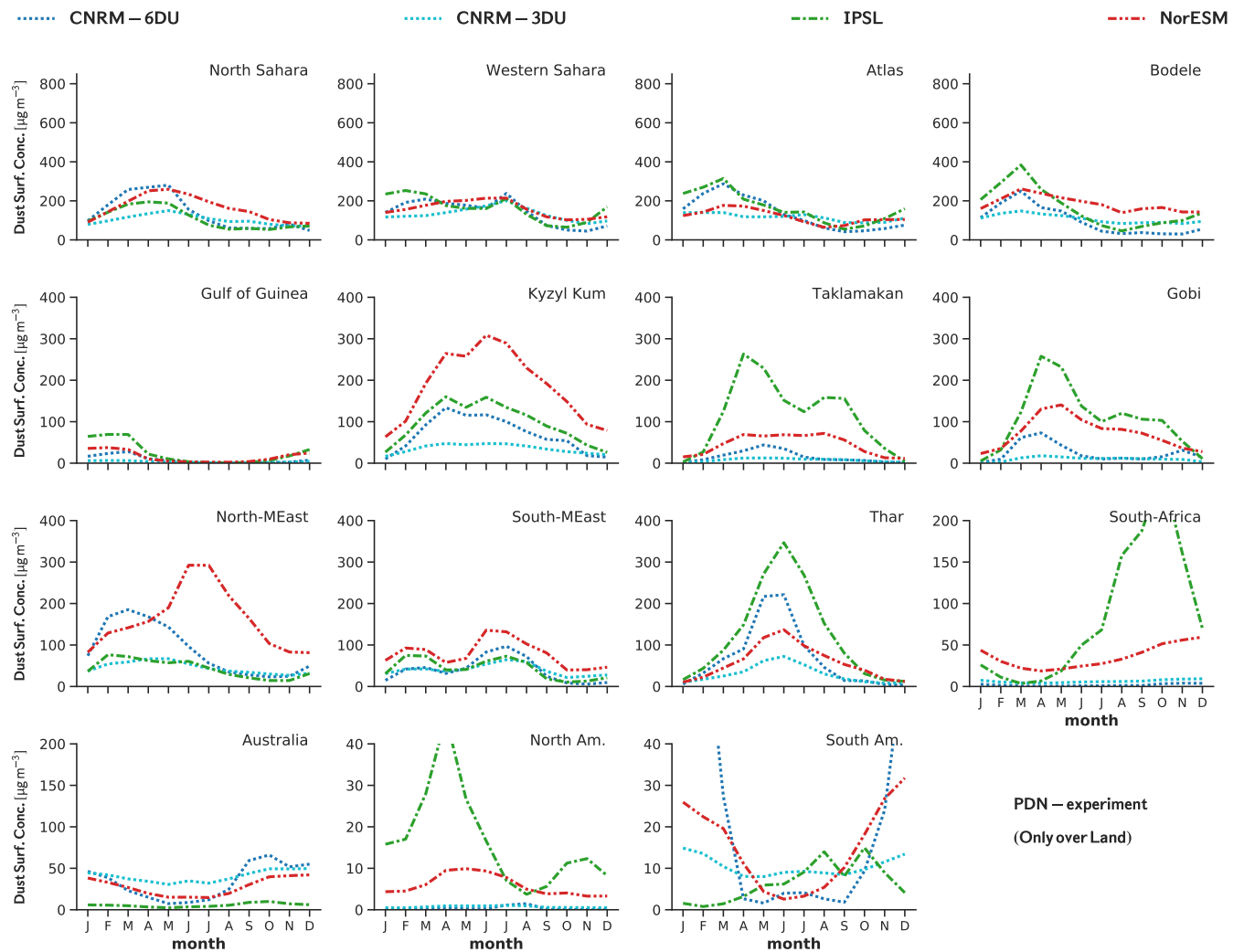


Figure S.DSC.5: The seasonal cycle of Dust surface concentration as modelled by CRESCENDO-ESMs for 15 regions. PDN experiment.

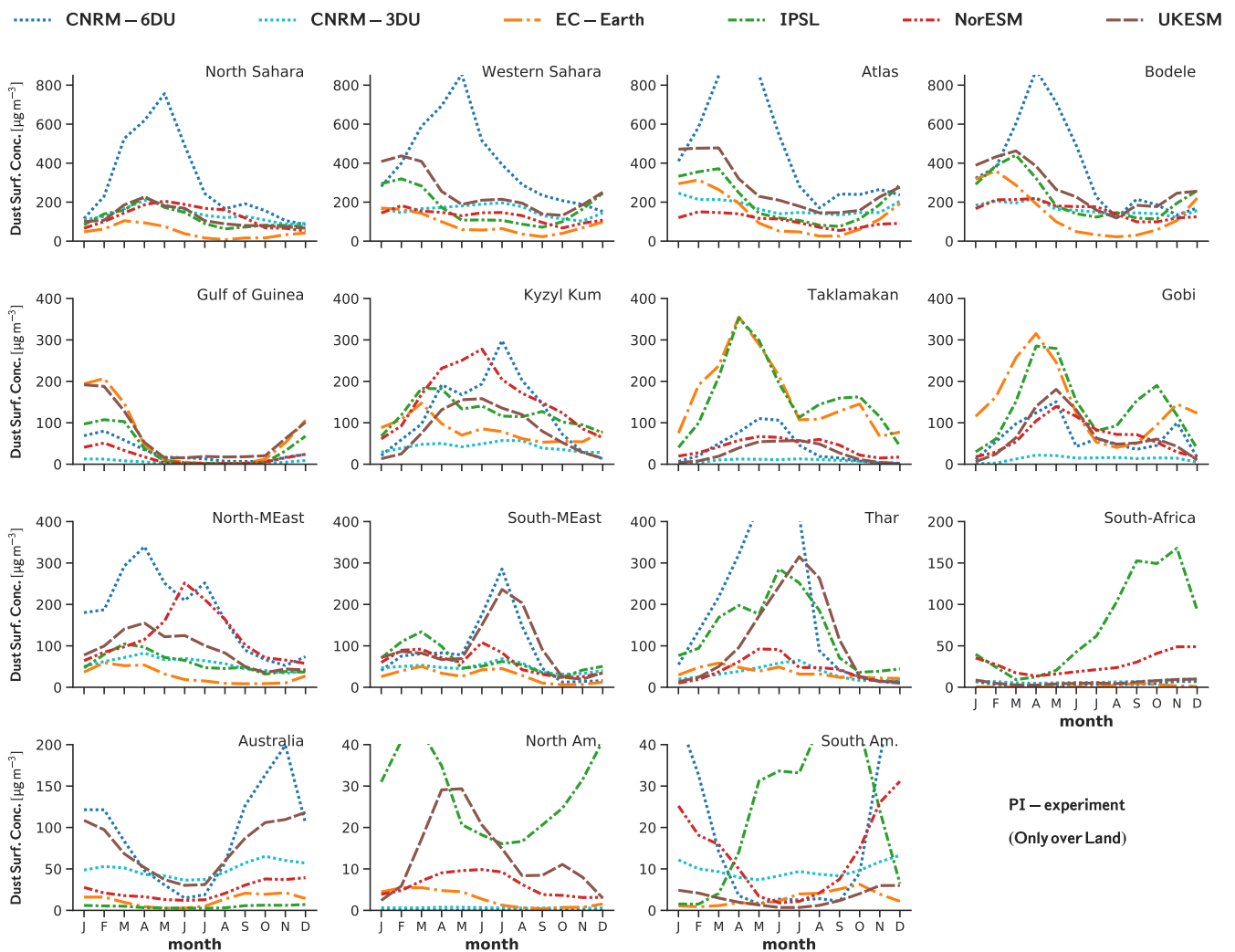


Figure S.DSC.6: The seasonal cycle of Dust surface concentration as modelled by CRESCENDO-ESMs for 15 regions. PI experiment.

Seasonal Cycle of Surface Conc. comparison with climatological dataset

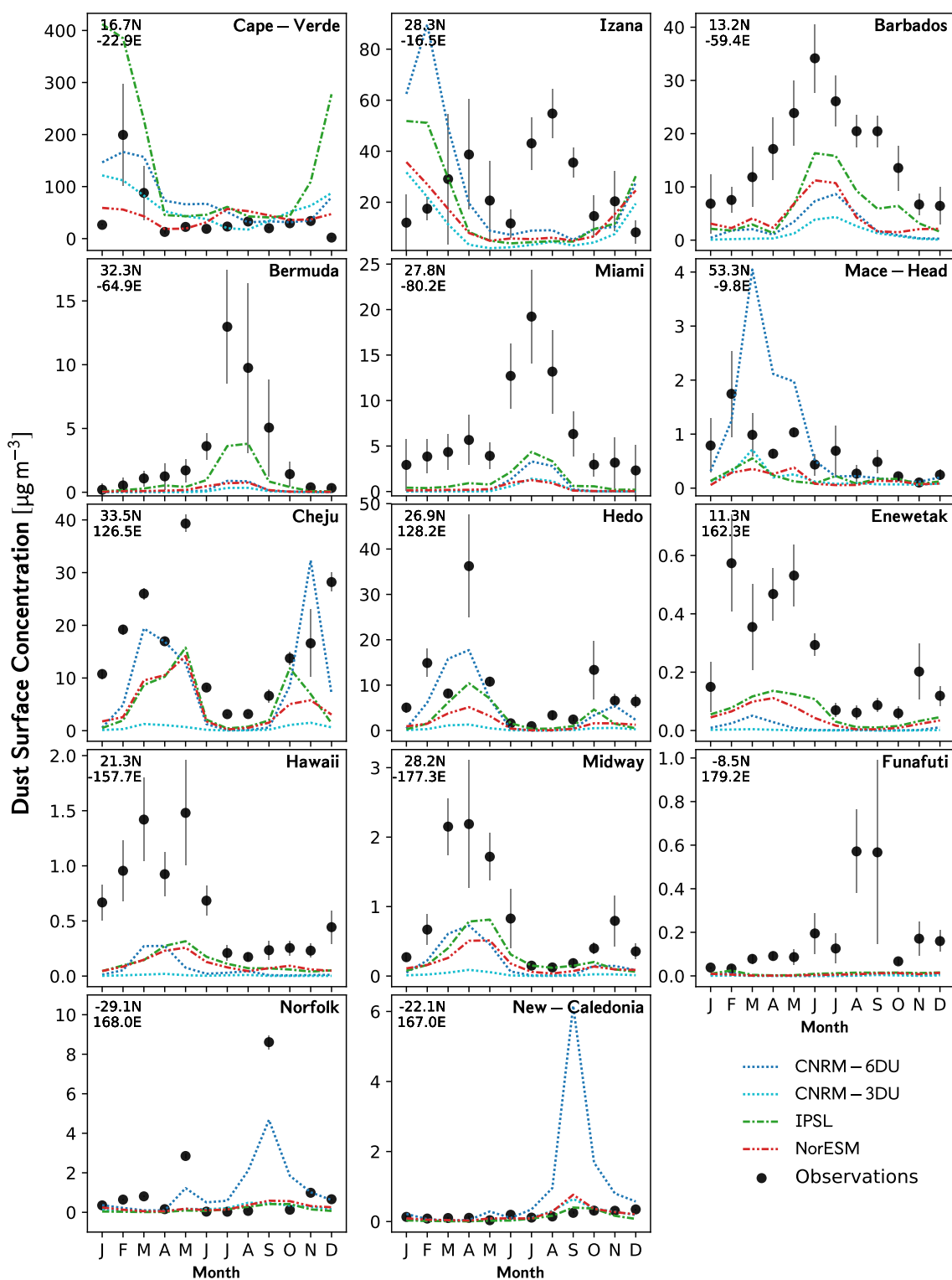


Figure S.DSC.7: Comparison of ESM models (PDN) of dust surface concentration with a station based climatological dataset.

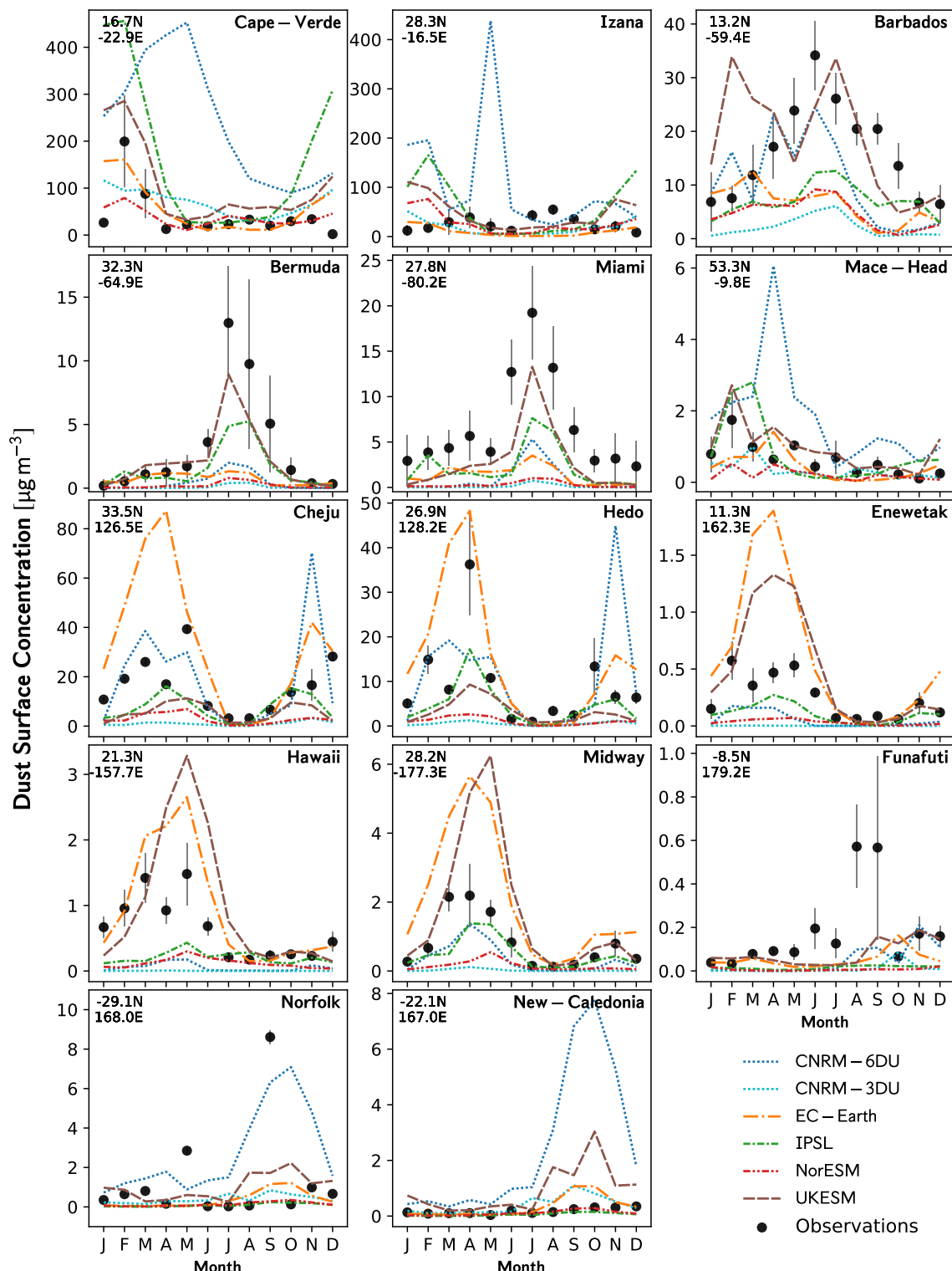


Figure S.DSC.8: Comparison of ESM models (PI) of dust surface concentration with a station based climatological dataset.

Network of Surface Concentrations

Model	Exp.	Surface Concentration Network					
		ρ	δ	δ_N	Σ	θ_N	η
CNRM-6DU	PD	+0.76	+23.19	+1.82	+4.59	+2.26	+65.14
CNRM-3DU	PD	+0.76	-2.46	-0.19	+1.52	+0.74	+16.92
ECv3	PD	+0.88	-0.48	-0.04	+1.92	+0.79	+24.36
IPSL	PD	+0.91	+8.53	+0.67	+3.03	+1.26	+38.95
NorESM	PD	+0.87	-5.62	-0.44	+0.84	+0.48	+9.95
UKESM	PD	+0.84	+8.08	+0.63	+3.88	+1.30	+54.14
CNRM-6DU	PI	+0.78	+28.15	+2.20	+5.27	+2.62	+76.81
CNRM-3DU	PI	+0.76	-2.22	-0.17	+1.56	+0.76	+17.54
ECv3	PI	+0.87	-0.73	-0.06	+1.76	+0.74	+22.15
IPSL	PI	+0.91	+8.58	+0.67	+3.06	+1.24	+39.12
NorESM	PI	+0.86	-5.64	-0.44	+0.84	+0.48	+9.85
UKESM	PI	+0.84	+8.26	+0.65	+3.96	+1.33	+55.34
CNRM-6DU	PDN	+0.87	+1.33	+0.10	+1.70	+0.86	+18.59
CNRM-3DU	PDN	+0.82	-5.36	-0.42	+1.08	+0.68	+13.98
IPSL	PDN	+0.89	+1.69	+0.13	+2.15	+0.98	+25.91
NorESM	PDN	+0.86	-4.58	-0.36	+0.95	+0.55	+11.72

Table S.DSC.9: Statistical properties of the evaluation of the CRESCENDO-ESMs dust surface concentration with respect to surface concentration networks. Statistics metrics are described in Table 4 of main paper.

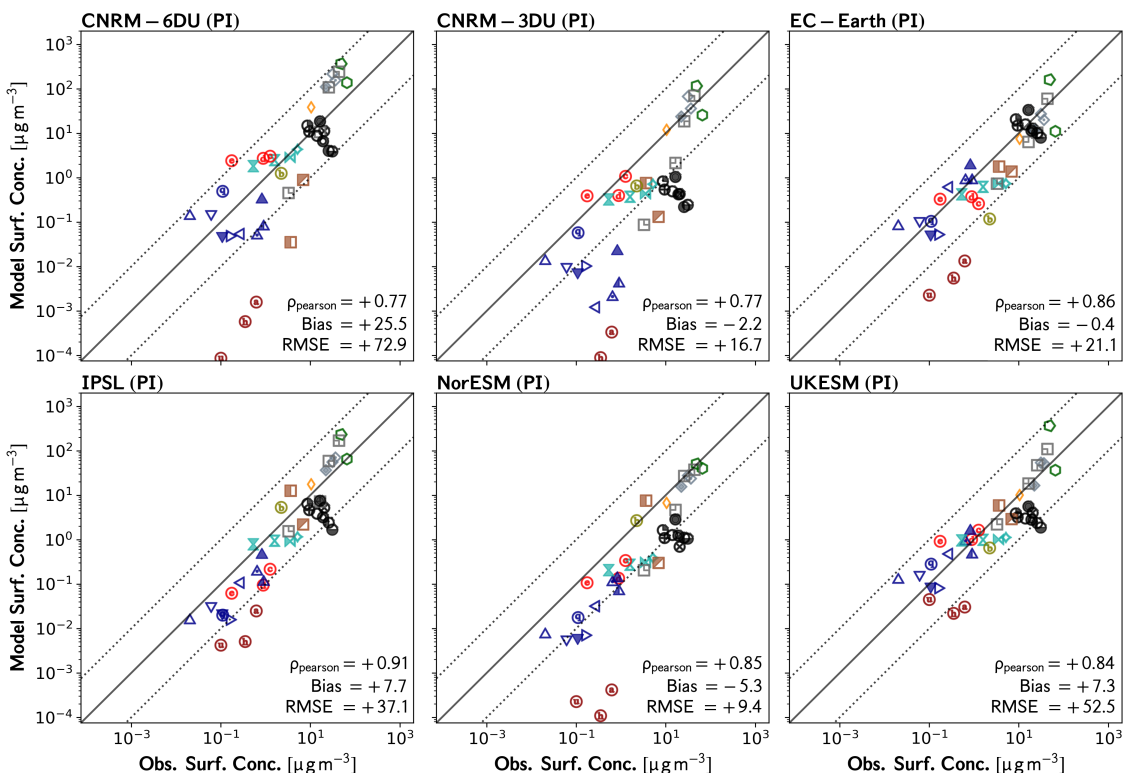


Figure S.DSC.10: Comparison of ESM models of dust surface concentration with a climatological dataset [1, 2]. The colors of the points are encoding the region where the measurement station. Climatological dataset obtained from observations 1991–1994.

References of supplement Dust Surf. Conc. (DSC)

- [1] Joseph M. Prospero and Ruby T. Nees. “Impact of the North African drought and El Niño on mineral dust in the Barbados trade winds”. In: *Nature* 320.6064 (Apr. 1986), pp. 735–738. DOI: 10.1038/320735a0. URL: <https://doi.org/10.1038/320735a0>.
- [2] Joseph M. Prospero and Dennis L. Savoie. “Effect of continental sources on nitrate concentrations over the Pacific Ocean”. In: *Nature* 339.6227 (June 1989), pp. 687–689. DOI: 10.1038/339687a0. URL: <https://doi.org/10.1038/339687a0>.